Journal of Hydrology 409 (2011) 663–681

Contents lists available at SciVerse ScienceDirect

Journal of Hydrology

journal homepage: www.elsevier.com/locate/jhydrol

Simulating the transition of a semi-arid rainfed catchment towards irrigation agriculture

A.J. Pérez [a], R. Abrahão [b], J. Causapé [c], O.A. Cirpka [a], C.M. Bürger [a,*]

[a] Center for Applied Geoscience, University of Tübingen, Sigwartstr. 10, 72076 Tübingen, Germany
[b] University of Zaragoza, Pedro Cerbuna 12, 50009 Zaragoza, Spain
[c] Instituto Geologico y Minero de España (IGME), C/ Manuel Lasala N 44, 9B, 50006 Zaragoza, Spain

ARTICLE INFO

Article history:
Received 22 December 2010
Received in revised form 21 April 2011
Accepted 29 August 2011
Available online 10 September 2011
This manuscript was handled by Philippe Baveye, Editor-in-Chief, with the assistance of Corrado Corradini, Associate Editor

Keywords:
Land-use change
Physics-based models
Transient simulation
Irrigation agriculture
Hortonian runoff
Dunne runoff

SUMMARY

We investigate the effects of land-use change in the semi-arid Lerma basin (Ebro valley, Spain), which underwent a transition from rainfed towards irrigation agriculture. For four consecutive years, this transition of formerly uncultivated land to irrigated farmland was intensively monitored. We use the calibrated and validated, physics-based, 3-D fully-coupled model HydroGeoSphere to study the hydrological effects of the change for this unique site, where spatio-temporal data on cropping patterns, irrigation and fertilizer amounts, and the associated catchment response are available with comparatively high resolution. Validation results show that the physics-based model can simulate and predict the impact of the land-use transformation and irrigation on surface and subsurface flow dynamics with high accuracy. Sensitivity and correlation analyses about the calibrated model parameter vector indicate that the set of van Genuchten parameter values and hydraulic conductivities is identifiable and locally unique for the parameter zonation that was defined using information on lithological units and texture data. In order to indicate changes in the runoff generation process and catchment functioning, we analyze the evolution of the total stream length and the average infiltration capacity provided by the model. The results show that irrigation agriculture has raised the base level of the water table of the Lerma aquifer causing new portions of the drainage network to become perennial. Furthermore, we introduce an approximate infiltration capacity, analyze its evolution and study its effect on Hortonian overland flow. Due to the physics-based nature of the model we can obtain values for exfiltrating fluxes directly from the model and show that both, the approximate infiltration capacity curve and the contribution of exfiltration to stream flow are consistent in indicating a shift from Hortonian towards Dunne flow runoff generating processes triggered by the land-use change.

1. Introduction

In the last century, irrigated agriculture has expanded around the world by 480% (from 47.3 MHa in 1900 to 276.3 MHa in 2000). Nowadays it represents 18% (≈280 MHa) of the global croplands and projections – focusing exclusively on developing countries – claim a further increase of 20% (up to a total of ≈330 MHa) by 2030 (Scanlon et al., 2007). In semi-arid areas, irrigation fosters crop productivity and allows for intensification and diversification of agriculture. As a backdrop, irrigation consumes 90% of global freshwater (Shiklomanov, 2000) and degrades water quality by flushing nutrients into soils and aquifers.

In the central Ebro valley (northern Spain), agriculture represents the main use of water and the majority of agricultural production relies on irrigation. The immense amount of water needed is supplied by a well-structured man-made channel network, which is fed by reservoirs located up to 100 km north in the higher Pyrenees. In recent years, the total irrigation amount has increased constantly, which has led to increased efforts to study the effectiveness of irrigation practices. Spanish researchers have begun to monitor larger irrigation districts in detail. Studies in the Bardenas irrigation district, (i.e. Causapé et al., 2004; Causapé et al., 2006) suggest that the intensification of irrigation has caused a considerable increase in nitrate within the drainage network. This may put the sustainability of these agricultural practices at risk. Despite the ongoing efforts, more comprehensive studies to improve the understanding of the impact of irrigation and land-use change on the surface–subsurface flow dynamics are still missing. One way to gain better insight in the latter could be by detailed modeling, where flow and transport processes are quantitatively described to a level consistent with available data series. Considering the ongoing land-use change where hydrosystems are forced by increasingly large amounts of irrigation water and cropping area expansion, we chose a physics-

* Corresponding author. Tel.: +49 7071 29 73173; fax: +49 7071 29 50 59.
E-mail address: claudius.buerger@uni-tuebingen.de (C.M. Bürger).

0022-1694/$ - see front matter © 2011 Elsevier B.V. All rights reserved.
doi:10.1016/j.jhydrol.2011.08.061

based, fully-coupled model to study the transition of a semi-arid rainfed catchment towards irrigation agriculture in detail.

By a physics-based model we refer to a model of coupled partial differential equations derived from the principles of conserving mass and momentum of water. In particular these are the shallow-water equations for flow at the land-surface and in streams and the Richards equation for flow in the subsurface. Parameters appearing in the equations have a physical meaning at a particular scale and may be measured at this scale. However, in the transition to larger scales, parameters attributed to more coarsely defined units become effective values which cannot directly be measured, but must be obtained by model calibration where details of the unresolved variability needed for rigorous upscaling are missing. Still, the principles of conserving mass and momentum hold and the relevant flow processes are directly represented in a spatially distributed way.

Fully-coupled surface–subsurface flow modeling approaches were first introduced by Freeze and Harlan (1969), who presented a blueprint for a physics-based mathematical model of a complete hydrological system. Since then, many studies have used this concept to simulate rainfall-runoff relationships. VanderKwaak and Loague (2001) applied the Integrated Hydrology Model (InHM) (VanderKwaak, 1999) to the R-5 catchment ($\approx$0.1 km^2). In particular, they simulated two "Horton type" rainfall events (i.e. rainfall rates are greater than the infiltration capacity of the soil) with duration of 1.6 and 1.9 h. To evaluate the goodness-of-fit, simulated hydrographs at the outlet were compared to the observed hydrographs by calculating the root mean squared error. The subsurface response could not be evaluated as the data set of the R-5 catchment did not include hydraulic heads in the unsaturated or saturated zones. Despite the "Horton type" forcing of the system, they found that both, Horton and Dunne (i.e. saturation excess overland flow) streamflow generation processes, are important for the R-5 catchment. The Dunne mechanism dominates along the channel axis, while the Horton mechanism is dominant in areas of low permeability. Using InHM the authors could track dynamic wetting and drying histories of partial-source (a single streamflow generation process dominant) and variable-source areas (where both mechanisms play a role).

Panday and Huyakorn (2004) presented a physics-based spatially-distributed model with additional capabilities to account for agricultural features at the catchment scale, namely the *storage exclusion* based on the definition of an obstruction height term and the *depression storage* related to rill heights. They successfully tested their implementation on the so-called tilted V-catchment by direct comparison to solutions obtained with two traditional hydrological simulation codes: HSPF (Bicknell et al., 1993) and HEC-1 (US Army Corps of Engineers, USACE).

Kollet and Maxwell (2006) presented an alternative coupling approach where overland flow is simulated as a free-surface boundary condition of the physics-based model. It is based on the assumption of pressure continuity across the surface–subsurface interface. This approach was used by Maxwell and Kollet (2008) to quantify the effect of subsurface heterogeneity on Hortonian runoff generation and to identify settings where groundwater flow dynamics directly feed back to the land-surface-atmosphere energy exchange (Maxwell et al., 2007; Ferguson and Maxwell, 2011).

Studying lake-groundwater interaction in a glacial outwash terrain (area = $\approx$4 km^2; Boreal Plains of northern Alberta, Canada), Smerdon et al. (2007) reported a successful application of a physics-based model at the watershed scale. They found that, due to the transition from the frozen to the thawed state of riparian peat in summer, a seasonal time-dependence of saturated hydraulic conductivity and storage coefficient had to be incorporated in their model.

Kolditz et al. (2007) presented a regional hydrologic soil model (RHSM) and applied it to simulate groundwater recharge patterns at a regional scale for the Beerze-Reusel drainage basin (Netherlands). This investigation evolved into the proposal of an object-oriented concept for the numerical simulation of multi-field problems in coupled hydrosystems, the so-called *compartment approach* (Kolditz et al., 2008).

Li et al. (2008) studied the hydrological response of the Duffin creek watershed (area = $\approx$286.6 km^2) honoring eight different hydrostratigraphic subsurface units with the physics-based, surface–subsurface model HydroGeosphere (Therrien et al., 2008). Subsurface hydraulic head observations, taken during a reference period, were used to constrain the initial condition for the simulated three-dimensional hydrological response driven by daily precipitation as measured from April to December of the years 1986 and 1987. Calibrating seasonally variable parameters controlling evapotranspiration (based on Hargreaves and Samani (1985), Kristensen and Jensen (1975)) for the year 1986, they found that their simulated stream-flow matched the measured one for 1987 at four different gauging stations within the catchment reasonably well. The subsurface response was not assessed due to the lack of concurrent hydraulic head time-series data.

Considering both, surface and subsurface hydrological response at the watershed scale, Jones et al. (2008) applied the physics-based InHM model to simulate the response of the Laurel Creek watershed (Ontario,CA) (area = 75 km^2) to two discrete rainfall events with 420 and 900 h duration. Their results show moderate agreement in simulated and measured runoff as well as subsurface hydraulic heads, and demonstrate the dynamic nature of the interaction occurring between the surface and the subsurface hydrological regimes. Their overall conclusion is that fully-coupled, surface/variably-saturated subsurface models are applicable at the watershed scale and possibly at larger scales. Nevertheless, they emphasize the need for more studies with more comprehensive data in order to improve the state of the art of coupled surface–subsurface modeling.

Despite the above mentioned successful applications of physics-based models, objections to these types of models are widely discussed in the hydrological literature. Apart from the question of parameter identifiability, uniqueness, and the need for effective parameter values at larger scales, (e.g. Beven, 1993; Beven, 2001, 2002), the range of validity of Richards' equation has been posed as a problem of physics-based models: Downer and Ogden (2004), Vogel and Ippisch (2008), among others, have pointed out that consistency with the assumptions underlying Richards equation requires a high spatial resolution that also depends on soil type and the scale of heterogeneities. Recent work of Kollet et al. (2010) has shown, however, that such a refined resolution is possible even at catchment scale by the use of high-performance computing. In this study, we see Richards' equation as an effective law leading to appropriate system behavior rather than a fundamental soil-physical law.

An important reason for the use of a physics-based model lies in the nature of the hydrosystem under consideration. The Lerma basin ($\approx$7.0 km^2 in size), located at the south-eastern part of the Arba catchment, see Fig. 1 is a semi-arid, formerly fallow land, whose transformation into an irrigation agriculture catchment was closely monitored by Spanish researchers. Since October 2005, predefined plots were gradually opened to local farmers for cropping and irrigation agriculture. In conjunction with the transformation, irrigation water amounts, crop pattern, and fertilizer application were documented plot-wise and stream-discharge measured in 15-min intervals at the basin outlet. The amount of irrigated water is gauged at irrigation hydrants located at each plot and the logged data regularly checked for plausibility. Nitrate concentrations and electrical conductivity were measured at first in daily intervals

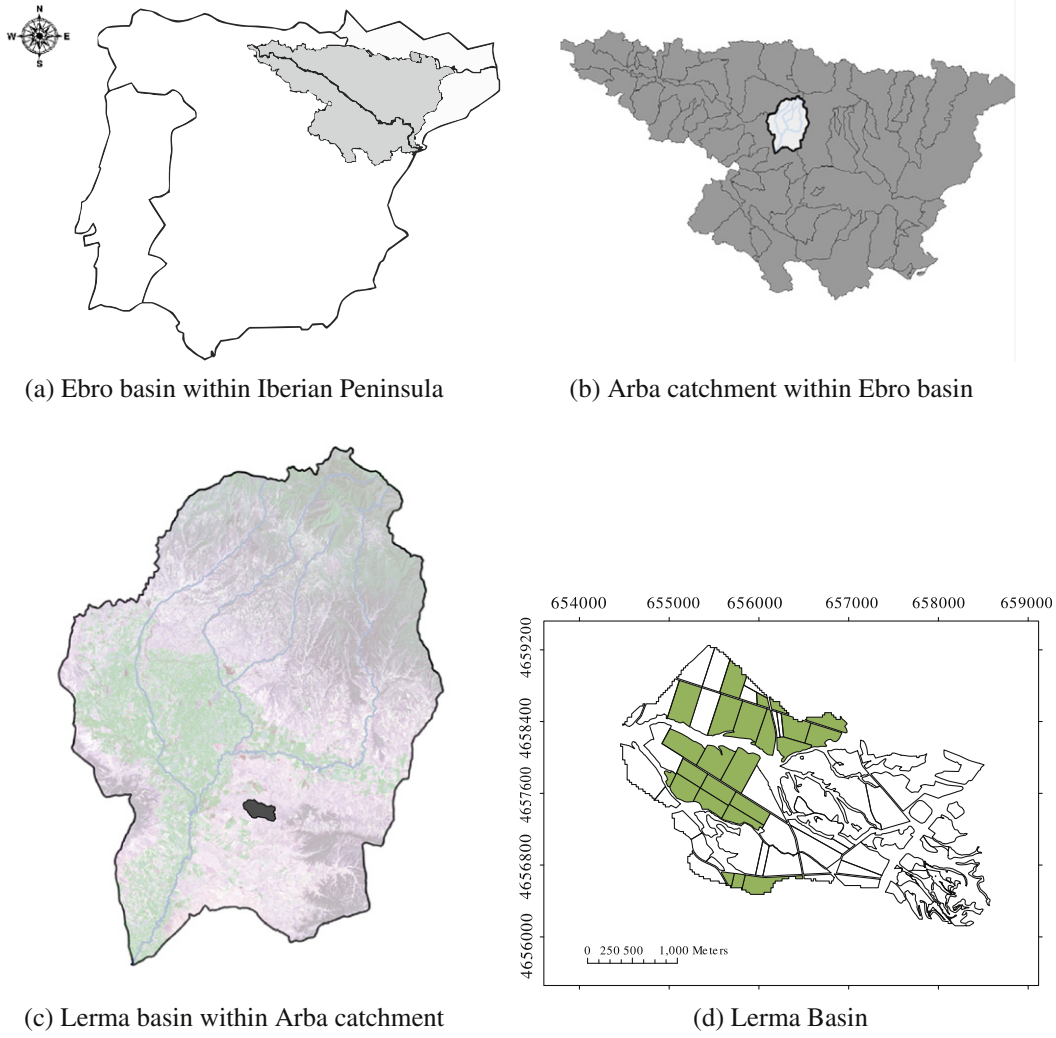

(a) Ebro basin within Iberian Peninsula

(b) Arba catchment within Ebro basin

(c) Lerma basin within Arba catchment

(d) Lerma Basin

Fig. 1. Location of study area in the Arba basin: (a) the Ebro basin within the Iberian peninsula; (b) the Arba catchment within the Ebro basin; (c) the Lerma basin within the Arba catchment and (d) the Lerma basin (the green areas represent irrigated plots for the hydrological year 2007). *Note:* Figures (a)–(c) are not drawn to scale. (For interpretation of the references to color in this figure legend, the reader is referred to the web version of this article.)

and since 2008 also in 15-min intervals at the basin outlet. Field observations comparing the hydrological year 2006 with subsequent years show that the intermittent main creek in Lerma basin has become a perennial stream due to irrigation. Considerable groundwater exfiltration is therefore evident. This indicates a shift in runoff generation processes during the monitoring period. We believe that such a situation, like shown in the study of Vander-Kwaak and Loague (2001), can adequately be modeled by coupled physics-based approaches. Furthermore, even though not an objective of this study, the long-term goal for the Lerma basin is the development of a model for the evaluation of the sustainability of current agricultural practices. In this context, the fate and transport of nitrate is of primary importance. The determination of surface–subsurface velocity fields and/or transient travel-time distributions are a prerequisite for transport simulation. Also the explicit consideration of the spatial distribution of transport parameters along different transport paths becomes important. Hence, a physics-based model was chosen.

The purpose of this study is to investigate the impact of the transformation of the semi-arid rainfed Lerma basin towards irrigation agriculture on the hydrological functioning of the basin. This study differs from others using coupled physics-based models by (1) the ongoing land-use transformation during the simulated period and (2) the strong influence of irrigation on the whole hydrosystem. Accounting for changes in land-use at this site is absolutely necessary for the reproduction of the changing surface–subsurface water flow dynamics.

2. Data inventory

The Lerma basin is geologically characterized by quaternary deposits on the lower part of a pediment. Subsequently we refer to these deposits as the "glacis" in slight abuse of the geomorphologic term referring to the sediment covered part of a pediment. The glacis consists of permeable, unconsolidated, clastic deposits that typically occur on pediments in arid or semi-arid climates and result from intense weathering and surface transport via episodic flow events. This glacis layer represents a shallow, phreatic aquifer that is seasonally fed by precipitation and irrigation return flows and discharges into the Lerma basin creeks. The glacis is overlying tertiary bedrock made up of lutites and marlstones. A locally used term for this formation is "buro" and we will adhere to it

hereafter. Causape (2002) indicated that the buro is relatively sensitive to weathering and fracturing processes so that water seepage through the upper buro layers is likely to occur. It is therefore assumed that water circulation through the top part of the buro does play a role for the subsurface part of the Lerma hydrosystem. Nevertheless, the buro unit as a whole represents an aquitard, so that we included only the top part of the buro unit into the model domain.

The very thin soil cover at Lerma basin consists of inceptisols, which only exhibit moderate to minor degrees of soil weathering and development. For this reason, we do not distinguish an explicit soil layer, but consider the glacis sediments and the negligible soil cover as a single model unit.

Beginning in October 2005, pre-defined plots (total area = 3.9 km^2) were transformed year by year into irrigated crop land. In the hydrological year 2006 (ranging from October 2005 to September 2006), 32% of these pre-defined plots became subject to irrigation (i.e. an area of 1.25 km^2). In the hydrological years 2007, 2008 and 2009 the proportion of the irrigated plots increased up to 68% (2.65 km^2), 80% (3.12 km^2) and 90% (3.5 km^2), respectively. The spatial pattern of this transition over time is depicted in Fig. 2. In the following, we will refer to the hydrological year by giving the number of the year, i.e. 2006, 2007, 2008 and 2009.

Topographic information of the Lerma basin is given by a digital elevation model (DEM) with a horizontal resolution of 25 m. The land-use patterns are defined by 60 surface units outlining the pre-defined plots (55 units), the creeks (1 unit), the non-irrigated areas (3 units), and irrigation water reservoirs (1 unit). In Fig. 3, the DEM is shown together with the surface unit polygons.

The climate of Lerma basin is classified by the Spanish Institute of Geomining Technology (SIGT) as Mediterranean warm climate (García-Garizábal et al., 2009) characterized by moderate to low rainfall (P = 450 mm) and high potential evapotranspiration (ETp = 1000 mm). The driest months correspond to Winter (December–January) and Summer (July–September) seasons and the rainiest to Spring (April–May).

Daily rainfall, air temperature, wind velocity, relative humidity and radiation are obtained from the climatological station Ejea de los Caballeros (operated by the Government of Aragon (Gobierno de Aragón)) located within 5 km from Lerma basin. In order to generate a reasonable hourly rainfall distribution for the Lerma basin (which is important for peak discharge simulation) the hourly rainfall distribution from the roughly 22 km distant climatological station Cola del Saso (operated by Confederación Hidrográfica del Ebro (CHE)) was used to distribute the daily totals measured at Ejea de los Caballeros over each 24-h period. As we found the 24-h sums of both stations to correlate well, this approach seemed to be justified. Stream discharge (Q) is measured at the basin outlet in 15 min intervals using a rectangular weir. Fig. 4 shows daily precipitation (P) and daily discharge (Q) series for the simulated period, i.e. the hydrological years 2006–2009. Based on hydroclimatological data, potential evapotranspiration is calculated with the well-known Penman–Monteith method (Beven, 1979; Penman, 1948). The reference evapotranspiration is calculated using grass as the crop reference (Allen, 2005; Allen et al., 1998). By a correction crop factor (k_c, see Table 1), we obtain the actual evapotranspiration. k_c values for each crop and each vegetative period were taken from Garcia-Vera and Martinez-Cob (2004) who studied actual evapotranspiration throughout the cultivated areas of the region. k_c values for baresoil were taken from Allen et al. (1998).

Considering the meteorological and agricultural patterns, we define three different seasons for the hydrological year (October to September) at Lerma basin: (i) non-irrigated season: the first 150 days -October to February- when comparatively small values of irrigation and precipitation are measured; (ii) rainy season: between March and mid-June when a high contribution of precipitation contrasts the much lower irrigation; (iii) irrigation season: mid-June to September, when predominantly irrigation takes place and precipitation is scarce.

In terms of subsurface observation data, hydraulic heads are available for eight piezometric wells located within the basin for 2008 and 2009 (see Fig. 5). However, due to technical problems piezometers 2 and 6 located very close to the northwestern and southern boundaries, respectively, were disregarded.

Porous media properties were obtained from a soil characterization campaign in the Bardenas district, which encompassed also 10 points with a sampling depth of 1.2 m within the Lerma Basin (see Fig. 5). The information consists of textures and bulk densities for the glacis unit. Porosities (ϕ) were indirectly calculated from bulk densities at saturated and dry conditions. Specific storage (S_s) and residual saturation (S_{w_r}) were defined from literature values (Freeze and Cherry, 1979). For the observed soil textures, typical values of saturated hydraulic conductivity (k_s) found in the literature (Carsel and Parrish, 1988) range between 0.005 and 1.0 m/d. However, values of k_s measured in pumping tests in the north of the Arba basin within the same lithologic unit (i.e. the glacis) are larger (between 1 and 7.7 m/d). Within the model calibration, we therefore used the extended range of values for the determination of effective saturated hydraulic conductivities. We use texture information and the corresponding ranges given in Carsel and Parrish (1988) to constrain the van-Genuchten parameters α and n for the glacis unit. Considering all texture classes identified in the Lerma basin, we allow ranges of α between 0.05 and 6.0 [m^{-1}] and of n between 1.01 and 2.0 [–]. Mean values ($\bar{x}$) and standard deviations (σ) from Carsel and Parrish (1988) for these textures are presented in Table 2.

3. Governing equations

In this section, we present the individual governing equations of the different flow processes within a hydrosystem as modeled by HydroGeoSphere (Therrien et al., 2008). As a starting point, however, we consider the basin scale water balance equation that may be used to obtain a first estimate of the change in storage inside the system by considering the difference of input and output flows per unit time:

$$\left[(PA_T) + \left(\sum_{j=1}^{N} I_j A_j\right) + Q_g - \left(\sum_{j=1}^{N} ET_j A_j\right) - Q_s\right] = (\Delta w_s + \Delta w_g) \quad (1)$$

where N is number of surface units (one for each land-use category); P is the total precipitation [L/T]; A_T is the total area of the basin [L^2], I is the irrigation rate [L/T] for each plot j with area A_j [L^2], Q_g is the groundwater inflow [L^3/T], Q_s is the discharge at the basin outlet [L^3/T], ET_j is the evaporation rate from the soil surface and subsurface along with plant transpiration [L/T] associated to each plot j, Δw_s and Δw_g are changes in surface water and groundwater storage [L^3/T].

In this study we use the water balance integrated over a hydrological year as a reference for the HydroGeoSphere model.

3.1. Overland flow

In the diffusive wave approximation of the Saint–Venant equations for overland flow, local and convective acceleration terms of the momentum equation are neglected and a hydrostatic vertical pressure distribution is assumed. By this, the flow velocity value corresponds to a vertical average. The approximation is generally applicable to mildly sloping streambeds. The diffusive wave equation can be written as follows (Gottardi and Venutelli, 1993):

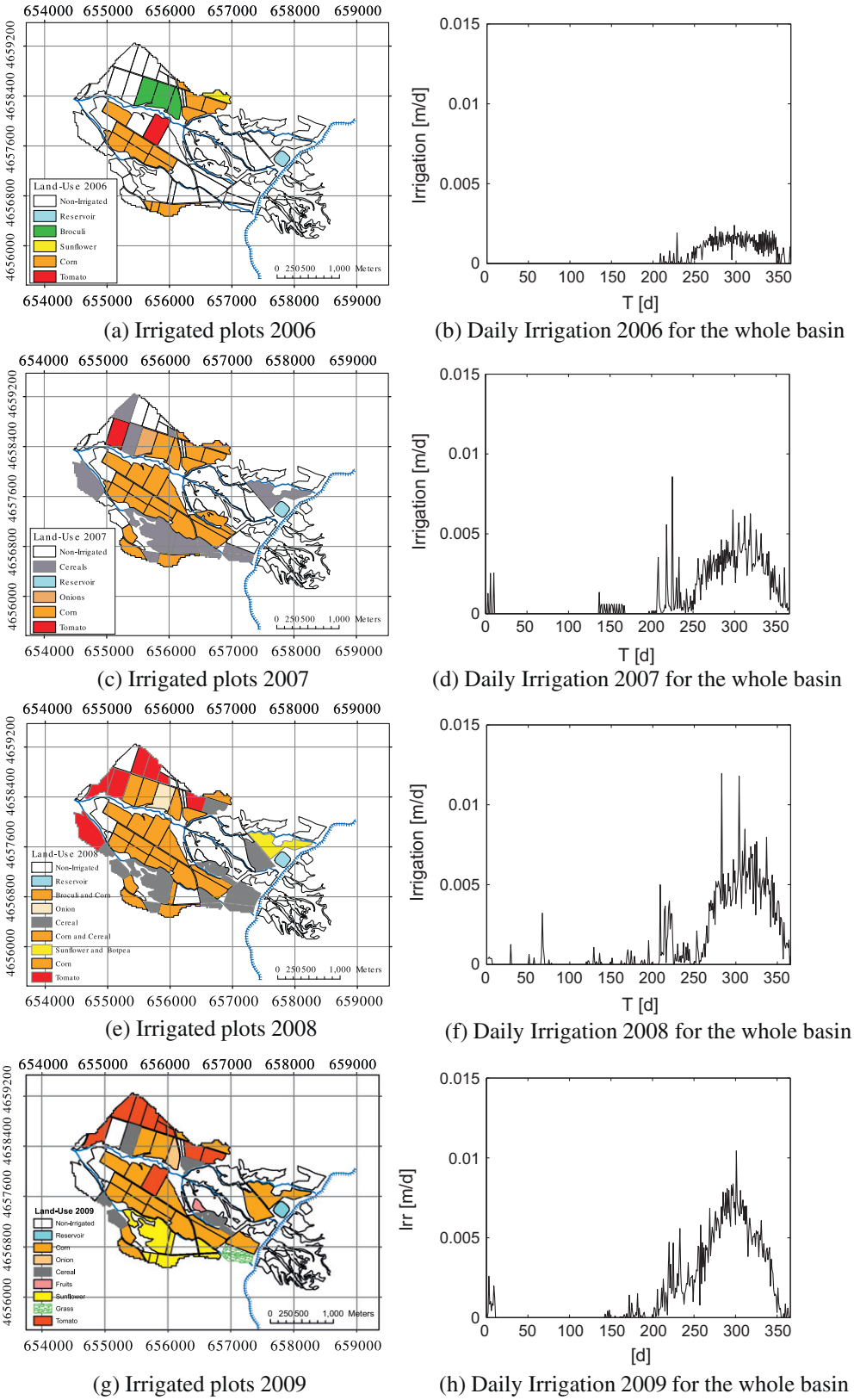

(a) Irrigated plots 2006 (b) Daily Irrigation 2006 for the whole basin

(c) Irrigated plots 2007 (d) Daily Irrigation 2007 for the whole basin

(e) Irrigated plots 2008 (f) Daily Irrigation 2008 for the whole basin

(g) Irrigated plots 2009 (h) Daily Irrigation 2009 for the whole basin

Fig. 2. Irrigated plots for the simulated years 2006–2009 and the corresponding daily amounts of irrigation for the whole Lerma basin. The coloring scheme represents the land-used for each year which includes baresoil, tomatoes, corn, cereal, and a label for a local reservoir lake.

$$\frac{\partial \phi_s h}{\partial t} - \frac{\partial}{\partial x_i}\left(Hk\frac{\partial h}{\partial x_i}\right) = -q^e \pm q_{og} \qquad \text{with } i \in \{1,2\} \tag{2}$$

in which we use Einstein's index notation implying repeated summation about each index appearing at least twice in a product. H is the water depth [L], h is the hydraulic head $(H+z)$ [L], z is the

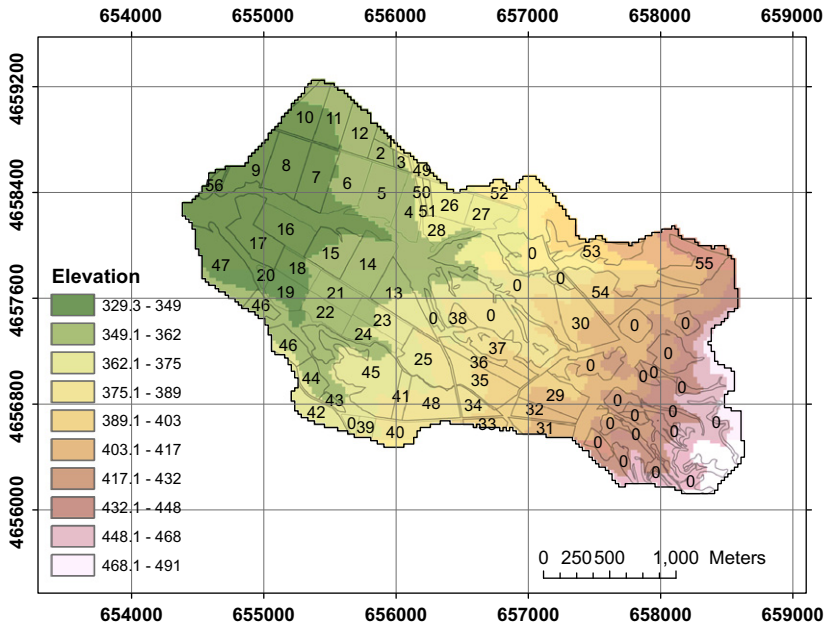

Fig. 3. Digital terrain model with the established surface units. Coloring scheme shows the distribution of the terrain elevation. Plots with zeros indicate the non-irrigable areas; plots with numbers between 1 and 55 show the pre-defined irrigable plots; and areas with no numbers represent the known creeks. (For interpretation of the references to color in this figure legend, the reader is referred to the web version of this article.)

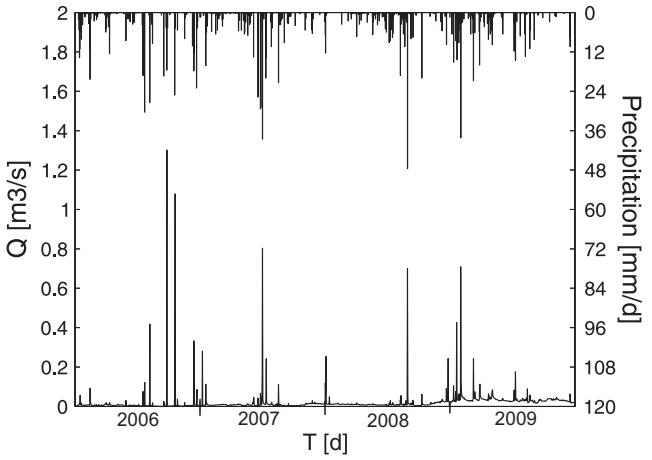

Fig. 4. Daily precipitation (top) and daily discharges Q (bottom) at the basin outlet for the simulated years 2006–2009.

bed elevation [L], q_{og} is a volumetric flow rate per unit area representing external sources and sinks (i.e. rainfall/evaporation) [LT^{-1}] and q^e is the surface-to-subsurface exchange rate [LT^{-1}], defined positive from the surface to the subsurface. ϕ_s [–] is the surface "porosity" introduced by Panday and Huyakorn (2004) to account for the effect of depression storage and obstructions on overland flow. To achieve this, the authors defined the height of depression storage (h_{ds}) and the obstruction height (h_{os}), which are physical parameters that can be interpreted as the mean spacing (equivalent void space) within the respective storage elements as a function of flow depth. k [LT^{-1}] is the surface conductance, here assumed isotropic, which can be approximated using Manning's equation after (Gottardi and Venutelli, 1993):

$$k = \frac{H^{2/3}}{n_m\left[\left(\frac{\partial h}{\partial x_1}\right)^2 + \left(\frac{\partial h}{\partial x_2}\right)^2\right]^{1/4}} \tag{3}$$

in which n_m [$TL^{-1/3}$] is Manning's friction coefficient.

Eq. (2) is subject to appropriate combinations of boundary conditions (no flow, fixed head, critical depth, normal depth).

3.2. Subsurface flow

Variably-saturated subsurface flow is modeled by Richards' equation expressed as:

$$S_w S_s \frac{\partial \psi}{\partial t} + \phi \frac{\partial S_w}{\partial t} - \frac{\partial}{\partial x_i}\left(k_{s_{ij}} k_{rw}(S_w)\frac{\partial h}{\partial x_j}\right) = 0$$
$$\text{with } i,j \in \{1,2,3\} \tag{4}$$

subject to:

$$n_i k_{s_{ij}} k_{rw}(S_w)\frac{\partial h}{\partial x_j} = \begin{cases} q^e & \text{at } z = z_{surf} \\ \pm q_g & \text{at lateral and bottom flux boundaries} \end{cases} \tag{5}$$

in which h is the total head of subsurface water, $k_{s_{ij}}$ is the saturated hydraulic conductivity tensor for the porous medium [LT^{-1}], k_{rw} is the relative permeability of the medium as function of water saturation (S_w) [–], ϕ is the effective porosity [–], q^e is the subsurface-surface exchange flux [LT^{-1}], q_g is the fluid exchange with the outside of the simulated domain through the bottom and lateral boundaries [LT^{-1}]; S_s is the specific storage [L^{-1}], ψ is the pressure head of water [L] given as $\psi = h - z$ where z is the elevation [L]. n_i is the normal vector at the land surface pointing upwards, and z_{surf} is the elevation of the ground surface. Eq. (4) may also be subject to Dirichlet or Cauchy boundary conditions with respect to hydraulic head.

In order to solve the non-linear Richards' equation for unsaturated flow, a relationship must be established between the primary unknown ψ and the secondary variables S_w and k_r, so that the latter two can be expressed in terms of the pressure head (ψ) (after Van Genuchten, 1980):

$$S_w(\psi) = S_{w_r} + \frac{1 - S_{w_r}}{(1 + (\alpha\psi)^n)^m} \tag{6}$$

Table 1
Monthly crop factors (k_c) for different common land-uses within the Lerma Basin Martinez-Cob (2004)

Crop	Monthly variation of the crop factor (k_c)											
	1	2	3	4	5	6	7	8	9	10	11	12
Baresoil	1.010	0.710	0.390	0.360	0.300	0.180	0.110	0.130	0.220	0.470	0.850	1.110
Alfalfa	1.010	0.710	0.370	0.920	1.010	0.950	0.920	0.920	1.160	0.470	0.850	1.110
Corn	1.011	0.707	0.392	0.308	0.309	0.647	1.173	1.222	0.781	0.394	0.849	1.110
WinterCereal	1.052	1.151	1.163	1.158	0.859	0.433	0.107	0.134	0.222	0.474	0.934	0.949
Rice	1.011	0.707	0.392	1.100	1.102	1.169	1.228	1.213	1.018	0.474	0.849	1.110
Grass	1.000	1.000	1.000	1.000	1.000	1.000	1.000	1.000	1.000	1.000	1.000	1.000
Sunflower	1.011	0.707	0.392	0.310	0.323	0.729	1.163	1.094	0.577	0.474	0.849	1.110
Pepper	1.011	0.707	0.392	0.306	0.336	0.676	1.033	1.071	0.969	0.474	0.849	1.110
Tomato	1.011	0.707	0.392	0.357	0.307	0.656	1.111	1.170	1.057	0.474	0.849	1.110
Onion	1.011	0.707	0.376	0.699	1.069	1.069	1.019	0.842	0.222	0.474	0.849	1.110
Broccoli	1.011	0.707	0.392	0.357	0.298	0.185	0.107	0.165	0.354	0.954	1.007	1.110
Peas	0.954	0.994	1.134	1.166	1.156	0.185	0.107	0.134	0.222	0.474	0.849	0.954
Trees	1.011	0.707	0.364	0.408	0.671	0.938	0.987	0.987	0.872	0.378	0.849	1.110
Barley	1.031	1.155	1.159	1.106	0.705	0.356	0.107	0.134	0.222	0.810	0.810	0.858
Oats	1.052	1.151	1.163	1.158	0.859	0.433	0.107	0.134	0.222	0.474	0.934	0.949
Cereal-Broccoli	1.052	1.151	1.163	1.158	0.859	0.433	0.107	0.165	0.354	0.954	1.007	1.110
Cereal-Sorghum	1.052	1.151	1.163	1.158	0.859	0.433	1.173	1.222	0.781	0.394	0.934	0.949
Cereal-Sunflower	1.052	1.151	1.163	1.158	0.859	0.433	1.163	1.094	0.577	0.474	0.934	0.949
Cereal-Corn	1.052	1.151	1.163	1.158	0.859	0.433	1.173	1.222	0.781	0.394	0.934	0.949
Broccoli-Corn	1.011	0.707	0.392	0.308	0.309	0.647	1.173	1.222	0.781	0.394	0.849	1.110
Peas-Sunflower	0.954	0.994	1.134	0.310	0.323	0.729	1.163	1.094	0.577	0.474	0.849	0.954
Peas-Corn	1.011	0.707	0.392	0.308	0.309	0.647	1.173	1.222	0.781	0.394	0.849	1.110
Pinetree	1.010	0.710	0.360	0.410	0.670	0.940	0.990	0.990	0.870	0.380	0.850	1.110

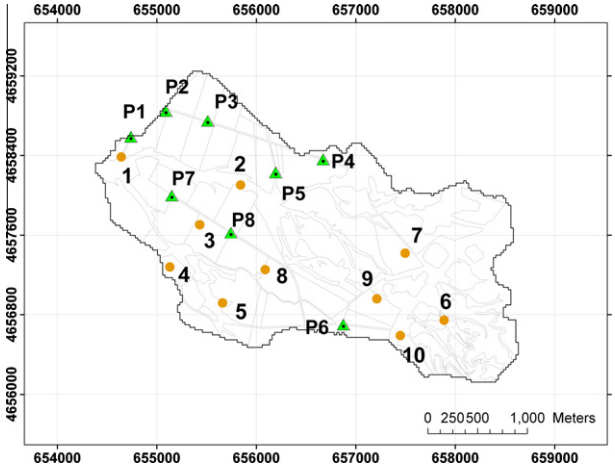

Fig. 5. Location of piezometers and soil samples. Triangles represent the available piezometers. Circles represents the soil samples: samples 4, 7, 9 were associated during the soil campaign to *clay* texture. Samples 1, 2, 5, 10 were classified as *clay-loam*. Finally, samples 3, 6, 8 were labeled as *sandy-clay-loam*.

Table 2
Soil hydraulic properties given in Carsel and Parrish (1988): saturated hydraulic conductivity (k_s), inverse air-entry pressure and pore-size factor (n).

Soil texture	k_s (m/d)		α (m^{-1})		n (–)		Samples no.
	$\bar{x}$	σ	$\bar{x}$	σ	$\bar{x}$	σ	
Clayey	0.05	0.10	0.8	1.2	1.09	0.09	4, 7, 9
Clayey–loam	0.06	0.17	1.9	1.5	1.31	0.09	1, 2, 5, 10
Sandy–clayey–loam	0.31	0.66	5.9	3.8	1.48	0.13	3, 6, 8

with S_{w_r} being the residual water saturation [–], α the inverse air-entry pressure [L^{-1}], n the pore distribution factor [–] and m defined as $m = 1 - 1/n$, $n > 1$. The relative permeability, k_{rw}, can be calculated as:

$$k_{rw}(S_w) = (S_e)^{1/2}[1 - (1 - S_e^{1/m})^m]^2 \qquad \text{with } S_e = \frac{S_w - S_{w_r}}{1 - S_{w_r}} \tag{7}$$

3.3. Surface–subsurface coupling

The surface flow equation is solved on a triangular 2-D finite element mesh on top of a matching subsurface prism grid, i.e. all x_1 and x_2 coordinates of the individual surface elements are the same for the corresponding subsurface elements. The surface flow equation Eq. (2) is coupled to the 3-D subsurface equation Eq. (3) via leakage through an interface layer. The surface nodes are connected to the first active subsurface flow nodes via a first-order relationship (i.e. the dual node approach) which can be expressed analogously to VanderKwaak (1999) as:

$$q^e = \frac{k_r k_{33}}{l_e}(\psi - H) \tag{8}$$

where k_r is the relative permeability for the exchange flux [–], k_{33} is the vertical saturated hydraulic conductivity [LT^{-1}] of the underlying porous medium and l_e is the interface layer thickness [L]. The relative permeability term k_r is the same as the relative permeability of the porous medium (k_{rw}) when water flows from the subsurface to the surface, while in the opposite direction, k_r is determined by the ratio of the water depth H at the surface to the total obstruction height ($h_s = h_{os} + h_{ds}$) (Panday and Huyakorn, 2004).

4. Model set-up

4.1. Discretization

The catchment model domain and zonation are shown in Fig. 6. The 3-D flow model of the Lerma basin is given by a finite element mesh of 141,943 nodes and uses a triangulation of the DEM as its top boundary, including mesh refinements along the known creeks. For the surface domain, 15,718 elements were assigned to 60 surface units representing the pre-defined plots. The maximum plan-view length scale of the elements is 40 m and the smallest elements located at the known creeks extend over 2 m. For the subsurface, we defined a two-layered geometry consisting of 235,770 prism elements. The top layer represents the glacis whose thickness varies in the irrigated area between 1.0 and 10.0 m; the bottom one represents the buro whose thickness varies between 1.0 and 4.0 m. Both layers are further divided into sub-layers.

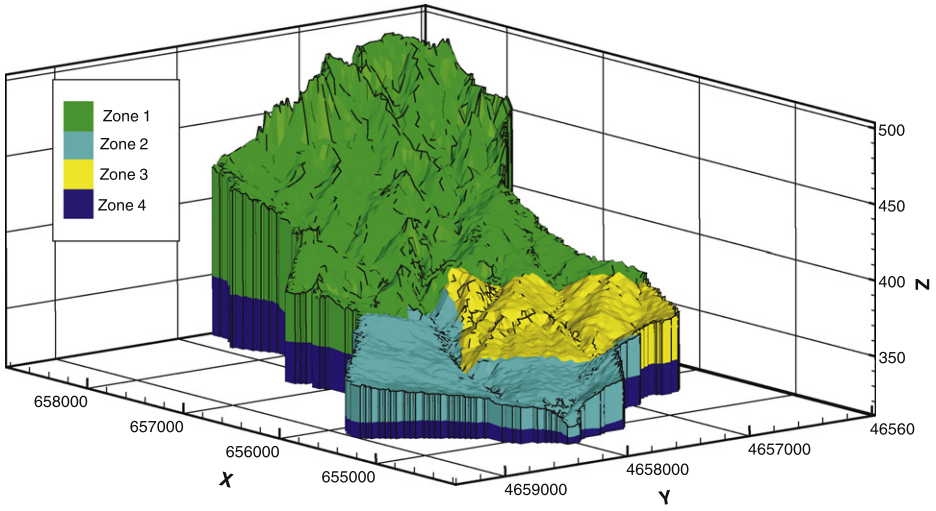

Fig. 6. Three dimensional representation of the hydro-stratigraphic units defined in Lerma basin. Zone 1: clay texture; Zone 2: clay-loam texture; Zone 3: sandy-clay-loam texture and Zone 4: buro.

The uppermost layer was subdivided into 0.1 m thick sub-layers in the top half and 2.0 m thick ones in the second half. The lower layer was subdivided into 5 sub-layers of varying thickness from 2.0 m to 10.0 m. To account for the spatial variability of soil parameters within the glacis layer a further zonation was introduced: (a) Zone 1: the western region of the basin characterized by clay texture; (b) Zone 2: eastern portion characterized by clay-loam texture; and (c) Zone 3: the middle of the basin characterized by sand-clay-loam texture . The buro layer was assumed to be uniform and labeled as Zone 4. Within each element, hydraulic conductivity was assumed to be uniform and isotropic. In the surface domain, we defined 60 different sub-domains corresponding to the land-use units. Actual evapotranspiration and irrigation amounts are set for each of these sub-domains separately. Manning's coefficients (n_m) are defined for each element according to the predominant land-use (see Table 3). Obstruction (h_{od}) and rill (h_{sd}) heights are both set to 0.002 m for the cultivated areas and to 0.0005 m for the non-cultivated areas. The coupling length required for the surface–subsurface exchange flow was assumed to be uniform for the whole domain and set to $l_e = (10^{-2}\ \mathrm{m})$ based on the work of Ebel et al. (2009).

4.2. Boundary conditions

For the surface domain, we defined the following boundary conditions: (a) time-varying boundary condition of the second-kind (Neumann) for the forcing fluxes (i.e. rainfall, evapotranspiration, irrigation); (b) boundary condition of the third kind (critical depth) at the lateral domain boundaries. The latter enforces a unique discharge flow-depth relationship, where the flow depth H equals the critical depth ($H = H_c$) and the relationship to the discharge per unit width at the boundary, Q_{eb}, can be expressed as:

$$Q_{eb} = \sqrt{gH_c^3} \tag{9}$$

The choice of the critical flow depth is supported by the fact that the gauging station at the basin outlet represents a weir, where critical flow is ensured. The upper boundary condition for the subsurface flow is given by the exchange fluxes through the interface layer to the surface as expressed in Eq. (8). We assume no-flow ($q_g = 0$) for the bottom and lateral subsurface domain boundaries due to the headwater characteristics of Lerma basin.

Table 3
Parameters for the predominant land-use within the Lerma basin: n_m: Manning coefficient; h_{ds}: the height of depression storage; h_{os}: the height of storage within the obstructions and l_e: coupling length.

Land-use	n_m (s/m$^{1/3}$)	h_{od} (m)	h_{sd} (m)	l_e (m)
Baresoil	0.03	2.0e−03	2.0e−03	0.01
Alfalfa	0.04	2.0e−03	2.0e−03	0.01
Corn	0.04	2.0e−03	2.0e−03	0.01
WinterCereal	0.04	2.0e−03	2.0e−03	0.01
Grass	0.04	2.0e−03	2.0e−03	0.01
Sunflower	0.04	2.0e−03	2.0e−03	0.01
Tomato	0.05	2.0e−03	2.0e−03	0.01
Onion	0.035	2.0e−03	2.0e−03	0.01
Broccoli	0.035	2.0e−03	2.0e−03	0.01
Peas	0.04	2.0e−03	2.0e−03	0.01
Trees	0.04	2.0e−03	2.0e−03	0.01
Barley	0.04	2.0e−03	2.0e−03	0.01
Oats	0.04	2.0e−03	2.0e−03	0.01
Roads	0.03	2.0e−03	2.0e−03	0.01
Major creeks	0.025	5.0e−04	5.0e−04	0.01
Secondary creeks	0.03	5.0e−04	5.0e−04	0.01
Pinetree	0.04	2.0e−03	2.0e−03	0.01

4.3. Initial condition

Ideally, the initial condition would be established from a comprehensive data collection campaign that provides the modeler with a snapshot of the system state at the beginning of the simulation period. Unfortunately, this true initial condition is hardly available for any catchment. Therefore, an initial condition was generated based on the concept of a dynamic water balance (e.g. Eagleson, 1978) The system is repeatedly forced with meteorologic input data (in this study: a one-year time-series of rainfall and evapotranspiration measured for the hydrological year previous to 2006) until the head distribution in the entire catchment does not change anymore when comparing a certain day of the current year with the same day of the previous year. The initial water table for this procedure was set coincident with the ground surface. For the hydraulic properties of surface and subsurface domains we used uniform parameter values for hydraulic conductivity and van Genuchten parameters, which were obtained from a preliminary study using a hillslope equivalent of Lerma basin (see Perez et al., 2010). Dynamic-steady state was reached after 20 years of forcing with the same one-year series. The discharge (0.030 m^3/s) for the 30th of September 2005 resulting from this procedure

was comparatively close to the average stream flow measured at the outlet of the Lerma basin over the first 40 days of the hydrological year 2006 (0.038 m^3/s). Fig. 7 depicts the total 3-D hydraulic head field for the initial condition.

4.4. Calibration

To match simulated and observed signals (i.e. calibration after (Anderson and Woessner, 1992)) for 2006, 2007 and 2008, we manually calibrated k_s, α and n for the different zones. We considered the root mean squared error (RMSE) and the Nash–Sutcliffe coefficient (N_r) as criteria for the goodness-of-fit. Automated calibration was not an option due to the long computation times of 9–12 h on an PC with a Intel Core 2 Duo E6600 2.4 GHz for a one-year simulation. The choice of the calibration parameters was based on the following: (i) no measured soil-retention curves were available, so that van-Genuchten parameters α and n could be only constrained by the texture information in combination with pedotransfer functions (Carsel and Parrish, 1988; Schaap and Leij, 1998; Schaap et al., 2001). (ii) no measurements of saturated hydraulic conductivity were available from inside the Lerma basin, but k_s measured outside the Lerma basin in the glacis unit were higher than the ranges obtained from the pedotransfer functions of Carsel and Parrish (1988); (iii) significant texture changes were observed within the glacis unit; (iv) a previous sensitivity study using a geometrical simplification of the Lerma basin showed a high impact of n, α and k_s on the simulated discharge dynamics (see Perez et al., 2010, for further information).

The model performance for both, surface and subsurface domains, was evaluated by visual comparison of time series of observed and simulated stream-discharge and subsurface hydraulic heads, as well as quantitatively by goodness-of-fit measures. Based on hourly discharge measurements at the outlet and the set of hydraulic heads measurements for the subsurface, we calculated the maximum error (ME), the root mean squared error (RMSE), the coefficient of residual mass (CRM), and the Nash–Sutcliffe coefficient (N_r). These statistics have previously been used to estimate residual errors and characterize systematic under and overpredictions, (e.g. Loague and Kyriakidis, 1997; Jones et al., 2008). RMSE represents an aggregated measure of model precision; CRM is the aggregated measure of the "deviation" of the predicted values in relation to the observed ones considering the sign of the deviation. The latter implies that both positive and negative deviations contribute to the calculation of CRM, thus in a well-balanced model the residual values should cancel out. In that respect, CRM represents a measure of model under- and overestimation. N_r is a typical statistic for assessing the goodness-of-fit of transient hydrological models.These performance measures are defined as:

$$\mathrm{ME} = max|S_i - O_i|_{i=1}^{n_{obs}} \tag{10}$$

$$\mathrm{RMSE} = \left[\frac{1}{n_{obs}}\sum_{i=1}^{n_{obs}}(S_i - O_i)^2\right]^{1/2} \tag{11}$$

$$\mathrm{CRM} = \frac{\sum_{i=1}^{n_{obs}}(O_i - S_i)}{\sum_{i=1}^{n_{obs}} O_i} \tag{12}$$

$$N_r = 1 - \frac{\sum_{i=1}^{n_{obs}}(S_i - O_i)^2}{\sum_{i=1}^{n_{obs}}(O_i - \overline{O})^2} \tag{13}$$

where S_i are the simulated values at measurement locations, O_i are the observed (i.e. measured) values, and n_{obs} is the number of observations.

For ME, RMSE and CRM the ideal value would be 0, whereas for N_r it would be 1. Negative values of CRM indicate a tendency of the model to overestimate discharge and hydraulic heads. Negative N_r indicate that the model prediction is worse than simply using the mean of the observations as a predictor.

Simulated and observed values for 2006, 2007 and 2008 are presented in Fig. 8. In general, they show good agreement. Peak flows are reproduced relatively well for the whole simulation period. For the non-irrigated season, the model is able to reproduce the measured flows adequately; however, for the year 2008 a minor tendency to overestimation is noticeable. For the rainy season, in particular for years 2007 and 2008, the highest peaks are slightly delayed. For the irrigation season, the simulated hydrograph captures the timing and the peak values relatively well. However, the most pronounced peaks are still underestimated.

As shown in Fig. 9, simulated water tables for 2008 match the measured hydraulic heads considerably well. Sharp increases of the water level at piezometers 3, 4 and 5 reflect the intensification of the irrigation during the second half of the year 2008. Hence, the model is able to reproduce the seasonal variation in the subsurface response.

The model performance statistics for the calibration period (years 2006, 2007 and 2008) are shown in Table 4.

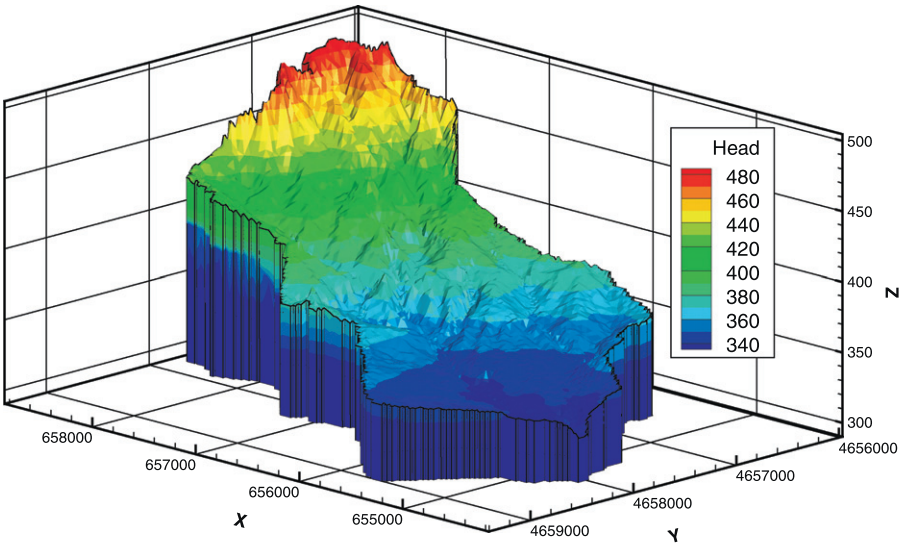

Fig. 7. Initial conditions used for the model simulations (at the beginning of the hydrological year 2006: October 1, 2005). Coloring scheme represents the total hydraulic heads obtained with the spin-up process. (For interpretation of the references to color in this figure legend, the reader is referred to the web version of this article.)

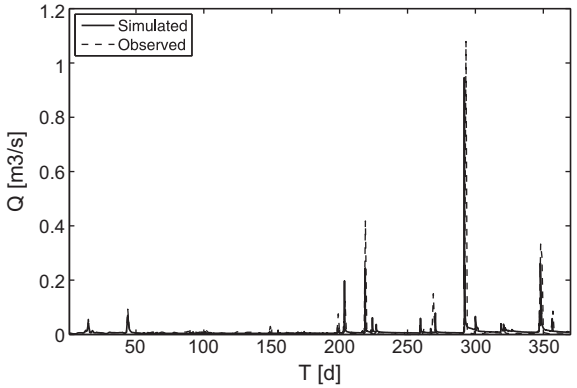

(a) Hydrological year 2006

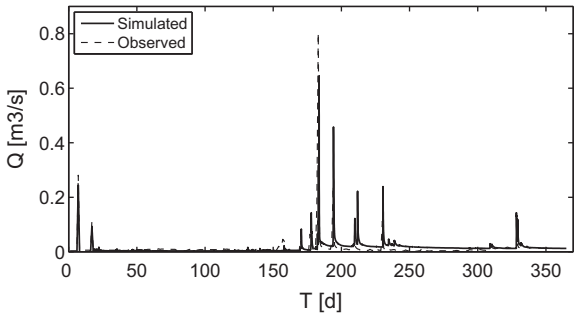

(b) Hydrological year 2007

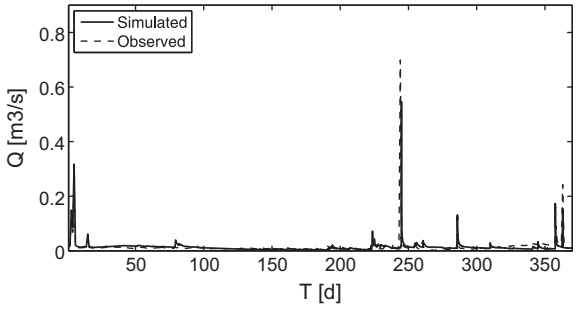

(c) Hydrological year 2008

Fig. 8. Simulated (solid) and measured (dashed) discharge for hydrological years 2006, 2007 and 2008. *Note*: The graphs are presented using different scales.

4.5. Validation

To validate the model, we used the data set for 2009. Hourly rainfall was available for this period directly from the station Ejea de los caballeros (within 5 km distance from Lerma basin) and used as the model input. No additional model parameter changes were applied. The integrated model was used for the prediction of discharge and groundwater heads for the entire Lerma basin.

We call this a prediction as the model is run with calibrated parameters, but using stresses (i.e. rainfall, irrigation and land-use) with markedly different conditions compared to the calibration period (Anderson and Woessner, 1992). As can be seen in Fig. 10, the model is able to reproduce the hydrological response of the surface domain despite the fact that also the size of the irrigated area increased again in 2009 (90% of the pre-defined plots are irrigated): peak and base flows are both represented very well, aside from a slight overprediction of stream discharge during the intensive irrigation phase. Simulated water tables match the measured hydraulic heads considerably well (Fig. 11). Only during the intensive irrigation phase the water tables are slightly overestimated. The performance statistics for the validation period (i.e. 2009) are integrated in Table 4.

5. Model assessment

5.1. Performance measures

Considering the performance results obtained from the calibration and validation, the following can be stated: The Nash–Sutcliffe coefficients, N_r, calculated for the calibration years 2007 and 2008, and for the validation year 2009 are very good (0.87, 0.86 and 0.90, respectively) which expresses the suitability of the model to simulate the hydrological response of the basin to the land-use transformation with respect to high and low flow timing. For 2006, the model efficiency is worse (0.64). This comparatively low value arises from the underestimation of the peaks during the rainy season. A source for this underestimation could be the high uncertainty of the actual short-term rainfall distribution within the Lerma basin. As discussed by Bronstert and Bárdossy (2003) the exact temporal variation of precipitation intensity and duration plays an important role for runoff generation, in particular for high-intensity rainfall events. These were very common during 2006, which was the rainiest year in the analyzed time period. Support for this hypothesis comes from the observation of the better performance obtained for 2009, when discharge was predicted using hourly rainfall available directly from the closer climatological station.

Small negative values of CRM for the years 2007, 2008 and 2009 reflect the tendency of the model to slightly overestimate discharge. Overestimation of both, the simulated stream discharge and subsurface heads may be caused by the assumption that the subsurface water divide coincides with the surface water divide, i.e. no lateral subsurface flow exists. There may also be a seasonal regional groundwater flow not considered in the model simulations, as the no-flow conditions assigned to the lateral subsurface boundaries force all water to leave the system at the surficial outlet, neglecting any kind of regional groundwater flow. This problem could be approached by the introduction of transient flux boundaries. However, additional field data would be required to quantify these boundary fluxes.

Another way to approach the influence of the regional groundwater flow could be the extension of the model domain beyond the watershed boundary to allow the water divides to develop "naturally". The success of this approach, however, will also depend on the quality of the characterization of the geometry of hydrostratigraphic units in the surrounding areas of the Lerma basin. As all characterization campaigns were focused more or less on the irrigated part of Lerma basin this approach was not followed.

Subsurface head mismatches may also be related to the uncertainty in the definition of the spatial variability of the hydraulic properties of the porous media within hydrostratigraphic units, but as geological information on internal heterogeneity is limited, the model was not made more complex to represent unit-internal variability.

In order to test whether our model is good in the sense that the deviations between the measured and simulated values are within the range of uncertainties (expressed by the error matrix $\mathbf{C_{mm}}$) we performed a χ^2-test of our objective function normalized by $\mathbf{C_{mm}}$ which can be expressed as:

$$\chi^2(\mathbf{p}) = \varepsilon^T \mathbf{C}_{\mathbf{mm}}^{-1} \varepsilon \tag{14}$$

where ε_i is the vector of errors consisting of n_{obs} entries $\varepsilon_i = o(\mathbf{x},t) - f(\mathbf{x},t,\mathbf{p})$, with $o(\mathbf{x},t)$ being the observation at location $\mathbf{x}$ and time t and $f(\mathbf{x},t,\mathbf{p})$ the simulated model output at the same location using model parameter vector $\mathbf{p}$. $f(\mathbf{x},t,\mathbf{p})$ can be a simulated

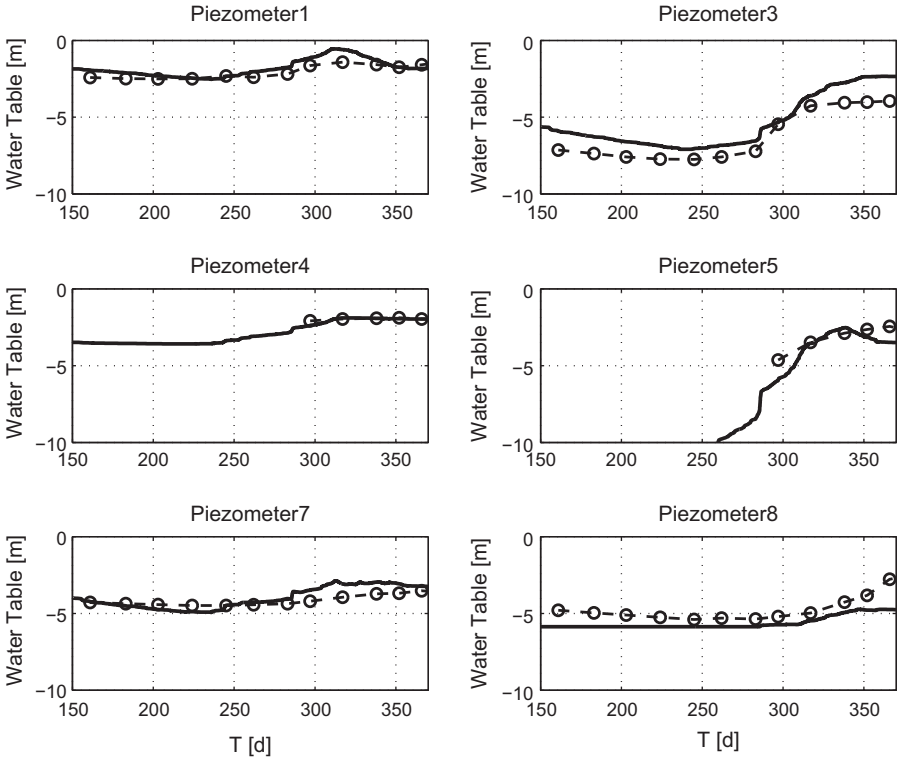

Fig. 9. Simulated (solid) and measured (dashed) groundwater tables for the hydrological year 2008. Piezometers 4 and 5 were dry during the first 7 measurements.

Table 4
Model performance statistics for the calibration period (hydrological years 2006, 2007, 2008) and the validation period (hydrological year 2009). ME: maximum error, RMSE: root mean square error; CRM: coefficient of residual mass; and N_r: the Nash–Sutcliffe coefficient.

Year	ME (m^3/s)	RMSE (m^3/s)	CRM (–)	N_r (–)
Calibration				
Surface				
2006	0.160	0.0136	0.60	0.639
2007	0.139	0.0417	−0.59	0.869
2008	0.066	0.0487	−0.18	0.857
Subsurface				
2008	1.50	0.68	0.0217	0.9322
Validation				
Surface	0.0737	0.0230	−0.09	0.901
Subsurface	1.35	0.75	0.0330	0.868

hydraulic head for the subsurface domain and a simulated discharge for the surface domain. χ^2 should be $\approx n_{obs} - n_{par}$ for the model to be acceptable. We assume that errors are uncorrelated, so that $\mathbf{C_{mm}}$ simplifies to a diagonal matrix containing the variance of the error for each observation on the diagonal. The error under consideration contains both, the aleatoric and the epistemic error or measurement and model error, respectively. More precisely, we can interpret the error as being the relative measurement error for stream discharge in the surface domain and the head measurement error, as well as the epistemic error due to the uncertainty in model structure and in boundary conditions for the subsurface. This kind of a decomposition would be consistent with the difference in available information regarding the surface and subsurface domain. To evaluate the performance of the model we ask for the maximum error that would allow us to accept our model in a χ^2-test. The analysis shows that a 12% relative error for the stream discharge and an error of 0.4 m (including head measurement error, uncertainty in model structure and boundary conditions) for the subsurface domain would be sufficient to pass the χ^2-test as the ratio $\varepsilon^T \mathbf{C_{mm}}^{-1} \varepsilon / (n_{obs} - n_{par})$ equated to $0.98 \approx 1.0$. These error values can be called very satisfactory for both domains, given that the 0.4 m for the subsurface also include the error in model structure and boundary conditions.

Finally, we can state that the model performance statistics obtained for both, surface and subsurface domains, show that our physics-based model has a high skill to reproduce the catchment flow dynamics during the land-use transformation.

5.2. Sensitivity analysis

Non-uniqueness and identifiability problems in the parameterization of physics-based models have been widely discussed in the literature (e.g. Beven, 1989; Ebel and Loague, 2006). Due to high parameter correlation between parameters, it remains difficult to obtain a unique set of parameter values in calibration. As reported by Maier et al. (2009), this is particularly problematic for van Genuchten parameters. In this study, we follow the definition of Ebel and Loague (2006) and distinguish between uniqueness and identifiability. We call a set of parameter values identifiable, if each individual parameter has an influence on the model output, i.e. the model output is sensitive to changes in each parameter evaluated about the set of calibrated parameter values. We call a set of parameter values unique, if the same optimal model performance cannot be achieved with another set of (different) parameter values. Uniqueness and identifiability can, but do not need to be related. By the following sensitivity analysis, we will explore identifiability and parameter correlation, which can also evaluate non-uniqueness about the set of calibrated parameter values. However, the question of global uniqueness or non-uniqueness in the sense defined above cannot be resolved by this analysis, as this would require such an analysis for every point of the entire parameter space.

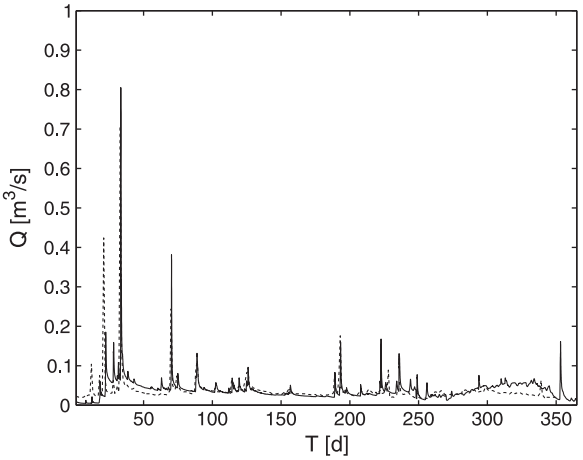

Fig. 10. Predicted (solid) and measured (dashed) stream discharge at the basin outlet for the hydrological year 2009.

Van Genuchten parameters were included in the calibration for the reasons explained in Section 4.4. Restricting the calibration to the physical ranges associated to texture classes identified for the Lerma basin, we found a set of values for α, n and k_s within Zones 1 to 4 deemed to be optimal.

In the following we calculate the sensitivity of each observation with respect to each parameter and use then to establish the covariance matrix of the parameters $\mathbf{C_{pp}}$ and the relative standard deviation of estimation σ_r [%] about the calibrated set of optimal values by linearized error propagation (e.g. Kitanidis, 1997).

Recalling that we defined $f = f(\mathbf{x}, t, \mathbf{p})$ as the model output at location $\mathbf{x}$ and time t given the vector of calibrated parameter values $\mathbf{p}$ (with a total of n_{par} values), an approximation of the sensitivity $\partial f / \partial p_i$ can be computed numerically using a forward-difference scheme (only observation locations and observation times are considered):

$$\frac{\partial f(\mathbf{x}, t, \mathbf{p})}{\partial p_i} \approx \frac{f(\mathbf{x}, t, \mathbf{p} + \delta_i \Delta p_i) - f(\mathbf{x}, t, \mathbf{p})}{\Delta p_i} \tag{15}$$

where δ_i represents an all zeros vector with a one at position i and Δp_i is a small perturbation of 1% of the value calibrated for parameter i.

We calculate the covariance matrix of the parameters $\mathbf{C_{pp}}$ about $\mathbf{p}$ from the covariance matrix of the measurement errors $\mathbf{C_{mm}}$ by linearized error propagation:

$$\mathbf{C_{pp}} = (\mathbf{J}^T \mathbf{C_{mm}^{-1}} \mathbf{J})^{-1} \tag{16}$$

with $\mathbf{J}$ being the $n_{obs} \times n_{par}$ sensitivity matrix containing all terms of the form $\partial f_i / \partial p_j$ calculated at observation locations and according observation times and n_{obs} the total number of observations considered in the calculation of $\mathbf{C_{pp}}$.

The main diagonal of $\mathbf{C_{pp}}$, calculated according to Eq. (16), contains the estimation variance σ_p^2 of each parameter p. It expresses the uncertainty in the determination of value of the calibration parameters. If σ_p is small compared to the value of p then the observations contain enough information and are sensitive enough on p to identify the value of p. Dividing the square root of σ_p^2 by the calibrated value of p, we obtain a relative standard deviation of estimation σ_r. σ_r-values for each parameter are shown on the main diagonal of Table 5. Except for α_2, the calculated σ_r-values are smaller than 10.0% indicating a low uncertainty in determination of the parameter values. In this sense, we may call the set of calibrated parameters identifiable.

Additionally, we also show in Table 5 the linear correlation coefficients r_{ij} ($i,j = 1, \ldots, n_{par}$) which can be calculated from the entries c_{ij} of $\mathbf{C_{pp}}$ (after Sun et al., 2001) by:

$$r_{ij} = c_{ij} / \sqrt{c_{ii} c_{jj}} \tag{17}$$

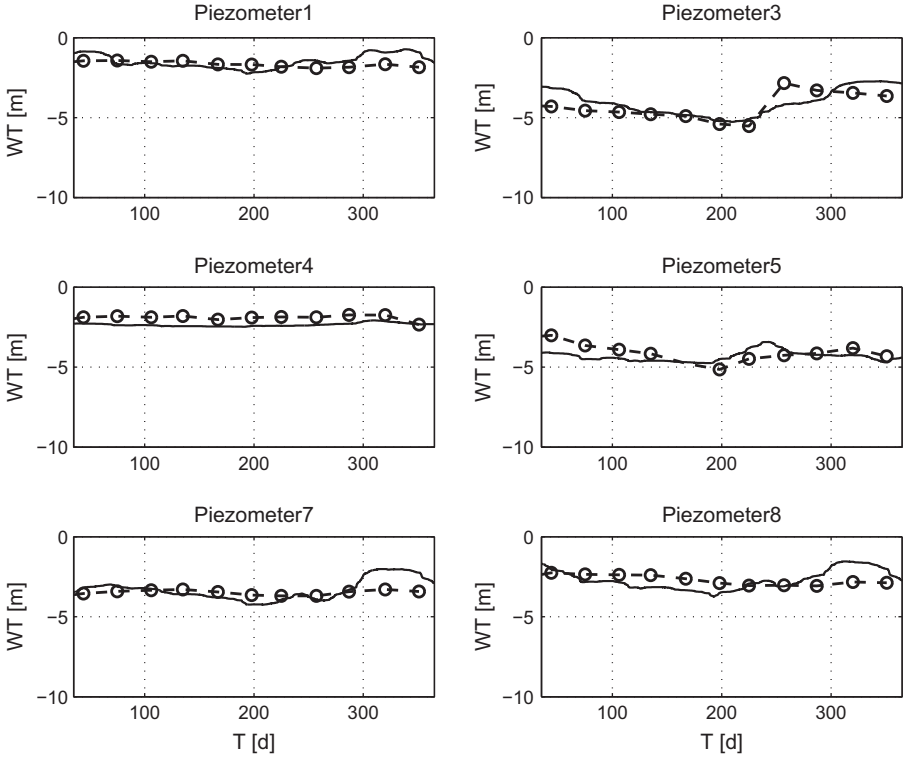

Fig. 11. Predicted (solid) and measured (dashed) water tables for the hydrological year 2009.

Table 5
Correlation coefficient r matrix calculated at the optimal values. On the main diagonal of the matrix we present the relative standard deviation of estimation σ_r (%). K_{s_i} (m/d): saturated hydraulic conductivity for the zone i; α_i (m^{-1}): van Genuchten inverse of air-entry pressure for the zone i; and n_i (–): van Genuchten pore-size factor for the zone i.

	K_{s_1}	α_1	n_1	K_{s_2}	α_2	n_2	K_{s_3}	α_3	n_3	K_{s_4}	α_4	n_4
Estimated value	0.9	0.01	1.09	4.5	0.5	1.31	6.5	5.9	1.72	0.9	2.0	1.39
Correlation calculated at optimal values												
K_{s_1}	7.94											
α_1	−0.033	11.19										
n_1	−0.415	0.719	1.21									
K_{s_2}	−0.223	−0.548	−0.193	1.52								
α_2	0.169	−0.023	−0.061	0.017	2.32			Symmetric				
n_2	0.280	−0.019	−0.139	−0.010	0.327	1.40						
K_{s_3}	−0.380	0.185	0.290	−0.109	−0.225	−0.162	1.17					
α_3	−0.249	−0.714	−0.469	0.332	−0.219	−0.133	0.031	1.25				
n_3	−0.073	−0.098	0.105	0.331	0.010	−0.067	−0.413	−0.280	3.98			
K_{s_4}	0.120	0.075	0.118	−0.036	−0.260	−0.262	0.175	−0.221	0.079	8.77		
α_4	−0.375	−0.166	−0.067	−0.068	0.102	−0.120	−0.259	0.311	−0.079	−0.658	3.44	
n_4	0.045	0.010	0.030	−0.079	0.327	0.300	−0.360	−0.125	0.079	−0.504	0.291	4.00

Standard statistics text books, e.g. Navidi (2008), consider a correlation coefficient r larger than 0.75 as indicative of a high linear correlation. In Table 5 we observe that none of the 66 values of r is higher than 0.75. The highest correlation coefficient ($r = 0.719$) was calculated between parameters α_1 and n_1. Also, the correlation coefficients obtained by this analysis quantify the correlation of parameter uncertainties rather than parameter values. That is, high values of r_{ij} do not indicate low identifiability if the corresponding relative standard deviations of estimation $\sigma_{r,i}$ and $\sigma_{r,j}$ are small. In summary, the above analysis shows that the calibration resulted in a set of parameter values which are identifiable and unique about the calibrated parameter vector. Given the results of the validation we can also state good predictive capabilities for the model.

6. Results and discussion

6.1. Water balance

Basin-scale water balances are the starting point of our analysis of the overall flow dynamics in the Lerma basin. We define the input as measured precipitation and irrigation amounts, and the output as estimated evapotranspiration and measured stream discharge, thereby neglecting possible measurement errors or limited representativeness of measurements. The contributions of precipitation and irrigation varied considerably within the simulation period: during 2006, irrigation represents 24.1% of the total amount of water input (the rest is precipitation). 2007 was drier in terms of precipitation (12.4% less than in 2006), while the total irrigation amount increased considerably (125.8% more relative to 2006). 2008 was drier than 2007 (21.3% less precipitation compared to 2007), but more irrigation took place (22.2% more than in the previous year). In 2009, irrigation increased by another 12.3% compared to 2008 (precipitation decreased by 17.4% compared to 2008). For the yearly water balance, we would assume that the change in water storage over the hydrological year is close to zero ($\Delta w_s + \Delta w_g \approx 0$). Furthermore, we assume that no water is entering or leaving the basin via lateral groundwater flow and that no water losses occur through the buro. Adhering to these assumptions, the left hand side of the water balance equation (Eq. 1) needs to equate to zero in order to close the water balance. If this is not the case (and lateral groundwater flow as well as water loss through the buro can still be ruled out), a negative value means that more water has left the basin than was introduced via precipitation and irrigation (which is equivalent to a release of water from storage), and a positive value means that the amount of water stored inside the basin must have increased by this value. The input and output terms as well as the water balances calculated for the years 2006–2009 are presented in Table 6. For 2006, the balance is slightly negative (−9.5 mm). In the following two years, during which irrigation increased considerably, the yearly water balances do not close either: compared to 2006 one order of magnitude of more water is stored inside Lerma basin (water balance values: +80.1 mm, +25.0 mm for 2007, 2008, respectively). In 2009, the balance is again slightly negative (−8.4 mm).

Table 6
Water balances for hydrological years 2006, 2007, 2008, and 2009.

Hydrological year	P (mm)	ET (mm)	Irrig. (mm)	Discharge (mm)	Water balance (mm)
2006	457.0	491.6	145.2	120.1	−9.5
2007	400.5	545.3	327.8	102.9	80.1
2008	315.1	582.9	400.6	107.8	25.0
2009	370.0	645.0	450.0	183.4	−8.4

This indicates that subsurface (and surface) storage cannot be neglected over a hydrological year for the period in which irrigation agriculture in the Lerma basin has intensified. Moreover, neither the discharge nor the pattern of the change in storage observed for the four years under observation does simply follow the (monotonically) increasing irrigation load. Therefore, we use the physics-based model for more spatially and temporally resolved analyses presented below.

6.2. Total length of streams within the Lerma basin

The first parameter analyzed with the physics-based model aims at changes of the drainage network. We calculated the evolution of the total length of streams, $\sum L$, in the Lerma basin. For this we considered the topographical setting of individual surface nodes (i.e. whether they are located in a valley) and defined a cut-off value of at least 10 cm water depth for a node to become a stream node. The evolution of the total stream length (see Fig. 12) shows that the additional input of irrigation waters over four consecutive years has indeed led to an increase of the length of the drainage network within the Lerma basin. Clearly observable are periods of increasing and decreasing total stream length over the hydrological year. For the first two years, irrigation did not result in a significant increasing trend of the total river length. Fig. 12 shows that for the years 2006 and 2007 the curve returns to essentially the same minimum level. In 2008, however, the pattern changes and the total river length does not return to the same level as in 2006 and 2007 instead it returns to a minimum level which is raised by roughly 600 m. This increasing trend seems to continue

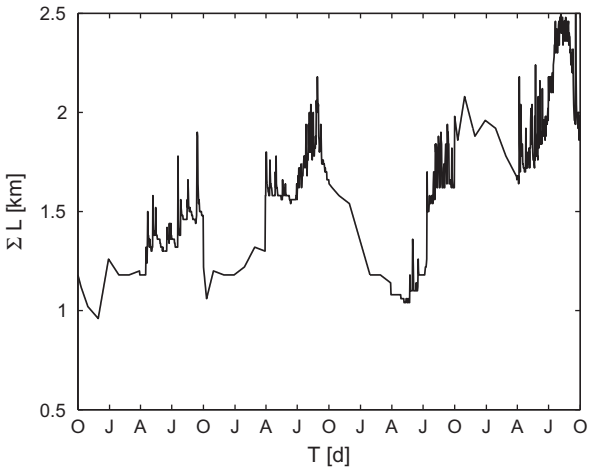

Fig. 12. Temporal evolution of the total length of the streams within Lerma basin.

for the year 2009 where the highest peak in total stream length is reached. Also the total river length never falls below the end level of year 2008, but rather returns to a minimum level which is again raised compared to 2008.

As observed in Fig. 12 the total stream length within Lerma basin has generally increased progressing transformation from rainfed to irrigation agriculture. The curve contains a seasonal trend induced by the rainy and irrigation seasons and some high-frequency fluctuations which we could identify (via the physics-based model) as the appearance of new intermittent creeks, that are mainly fed by quick irrigation return flow. It is interesting to notice that the input of irrigation waters in the first two years did not result in a significant increase of the total stream length over the whole year. As the total stream length curve returns to essentially the same base level of 1 km, it seems reasonable to interpret this as the proportion of the drainage network that represents perennial streams during 2006 and 2007. In 2008, apparently a threshold was reached as the total stream length does not return to the former base level at the end of 2008, and a new proportion of the drainage network becomes perennial. Looking at the basin-scale water balance, the high storage of water in 2007 and 2008 and the continued input in 2009 also seems to suggest that the Lerma system may now be able to sustain spring areas at a higher topographic level - at least in some parts of the basin. Indeed it has been observed in the field that the creek south of the main stream of Lerma basin is no longer falling dry during summer. Model inspection indicates that the additional stream length results from this stream branch becoming perennial.

6.3. Surface-runoff generation processes

The second parameter analyzed with the physics-based model aims at the shift in surface-runoff generation processes from Horton (infiltration excess, Horton, 1933) to Dunne (saturation excess, Dunne and Black, 1970) flow. Considering the complete spatial differentiation of soil moisture over time we calculated the temporal evolution of an average *approximate* infiltration capacity, $\overline{Q}_{cap}$, and the total water input rates, Q_{ri}, (i.e. rainfall + irrigation). Thereby $\overline{Q}_{cap}$ was obtained by integrating the unsaturated hydraulic conductivity of the top subsurface nodes over the whole surface area of the Lerma basin model taking spatial differences in saturation, van Genuchten parameters and saturated conductivity into account and normalizing by the surface area. Since the conditions for Hortonian runoff are given when the rainfall intensity exceeds the infiltration capacity of the soil (e.g. Dingman, 2002; Loague et al., 2010), it is expected that our approximate infiltration capacity is indicative for whether or not a certain rainfall event will generate Hortonian runoff at a particular model element. The actual infiltration capacity, however, changes during a rainfall event, such that our definition (at an hourly time step) can only represent an approximation of the actual infiltration capacity. We therefore call $\overline{Q}_{cap}$ an (average) *approximate* infiltration capacity. $\overline{Q}_{cap}$ should also not be confused with the empirically defined infiltration capacity for a catchment in "steady-state" at field-saturation (Betson, 1964):

$$\overline{Q}_{cap} = \frac{1}{A_{total}} \int_A k_{rw}(x, y, z_{surf}) k_s \mathrm{d}A \tag{18}$$

The integration given in Eq. (18) was repeated using 1-h time-step for the whole simulated period. The resulting curve is presented in Fig. 13. Considering the general trend of the curve we observe the following:

Values of $\overline{Q}_{cap}$ are relatively low for 2006 before irrigation starts. During this period Q_{ri} is often higher than the average approximate infiltration capacity. 2007 was drier in terms of total precipitation. Nevertheless, there are two distinct maxima of $\overline{Q}_{cap}$ observable, which are not time-related to the major irrigation phase. These two distinct maxima do not re-occur in the following years. Only

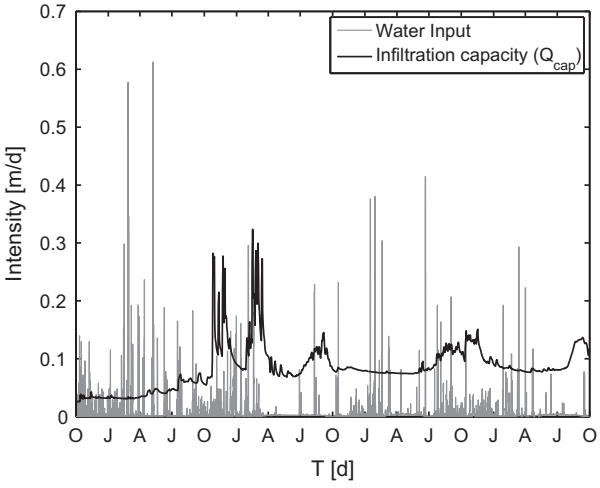

(a) Infiltrationcapacity, Q_{cap}

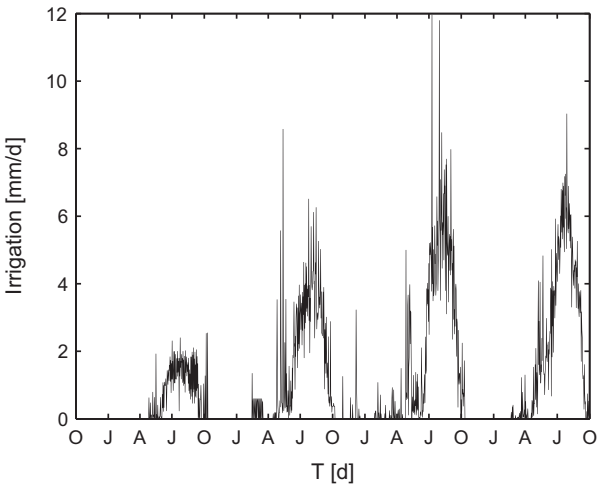

(b) Irrigation

Fig. 13. Temporal evolution of the infiltration capacity, Q_{cap}, of the Lerma basin.

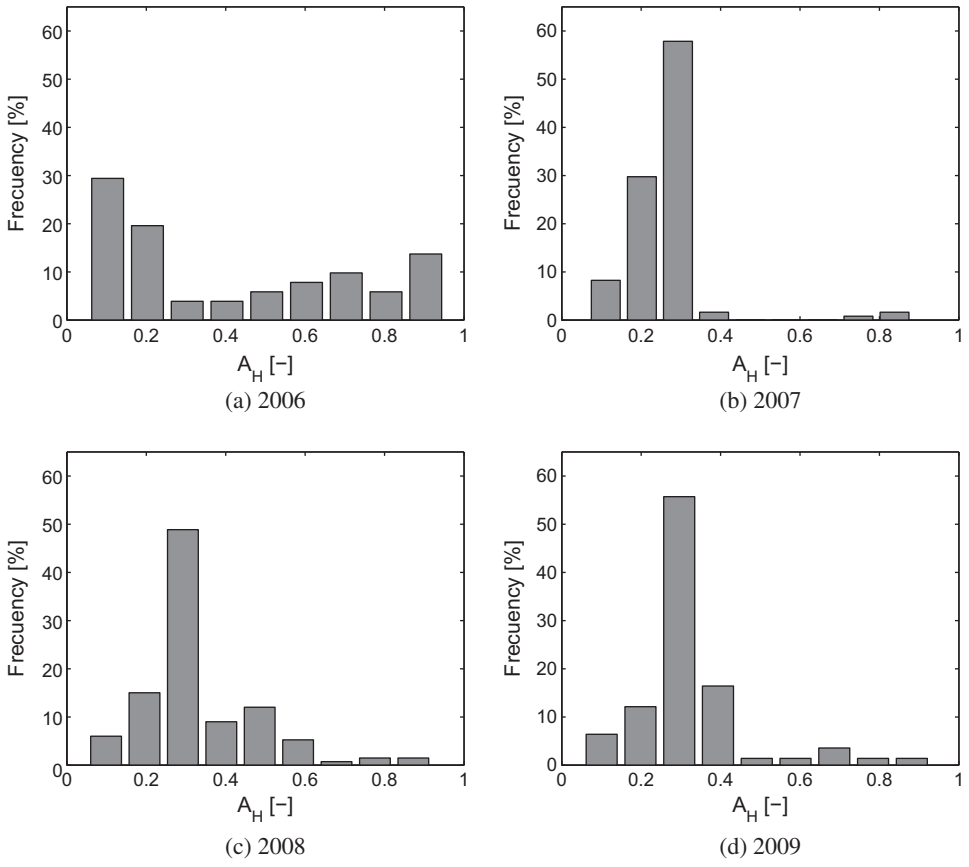

Fig. 14. Histograms of the proportion of areas associated to Hortonian runoff A_H generation (relative to total catchment area) for hydrological years 2006–2009.

within the rainy season and during a few events that the rainfall intensity Q_{ri} exceeds $\overline{Q}_{cap}$. Despite the increase of Q_{ri} during the irrigation season, Q_{ri} is never larger than $\overline{Q}_{cap}$. During 2008 the base level of $\overline{Q}_{cap}$ increased considerably, so that $\overline{Q}_{cap}$ is again exceeded only during a few extreme rainfall events. In the hydrological year 2009 the base level of $\overline{Q}_{cap}$ is larger than in all other years. Still for a few events in the second half of the year Q_{ri} exceeds $\overline{Q}_{cap}$. Additionally, one can observe that the major irrigation phases coincide with prolonged (local) maxima of $\overline{Q}_{cap}$ in 2007 and 2009.

The comparison of the evolution of $\overline{Q}_{cap}$ vs. Q_{ri} shows that in 2006 the conditions for Hortonian runoff, i.e. $Q_{ri} > \overline{Q}_{cap}$, are reached in about 24 events. During the next three years, conditions for Hortonian runoff are only reached in about 17 events in total. While this is partly due to differences in the rainfall distribution, it is also obvious that the higher base level of the average approximate infiltration capacity curve requires stronger rainfall intensities for Hortonian runoff generation. This suggests a shift in the runoff generation processes in the Lerma basin: from relatively regularly occurring Hortonian runoff in 2006, characterized by high discharge during rainfall events and followed by longer periods of zero overland flow, to a more Dunne flow dominated runoff generation process in the later years. Particularly interesting is the year 2007, where the approximate infiltration capacity curve has two distinct maxima from November 2006 to March 2007. During these two time periods water input by irrigation does not play a major role. However, the base level of the approximate infiltration capacity curve is already raised due to the irrigation phase in late 2006. The frequent precipitation events occurring during the two time periods in question (in 2007) are not too intense, but would have led to Hortonian runoff generation in early 2006. In 2007, however, the approximate infiltration capacity is just high enough to accommodate the rainfall at these rates and most of the rainfall contributes to soil wetting. We conclude that this is the reason for the two distinct maxima of $\overline{Q}_{cap}$ in 2007, which are not related to intensive irrigation. This conclusion is also supported by the characteristics of these maxima: they are only of short duration and fluctuating quite intensively, whereas $\overline{Q}_{cap}$ maxima induced by irrigation during later times show a comparatively smooth variability. The reason that the 2007 maxima type does not re-occur in later years is believed to be chiefly due to the non-recurrence of longer duration low intensity rainfall.

As the approximate infiltration capacity $\overline{Q}_{cap}$ represents only an average value for the total Lerma basin area, it does not account for local differences in runoff generation. In order to also include these in our analysis, we determined the total area with Hortonian runoff generation (i.e. $Q_{ri} > Q_{cap}$) based on the individual contributions from each model element. The latter is achieved by computing the relative area of Hortonian runoff generation A_H as:

$$\overline{A}_H = \frac{1}{A_{total}} \int_A I(Q_{ri} > Q_{cap}) \mathrm{d}A \tag{19}$$

where I is a function which is set to 1 when the property $Q_{ri} > Q_{cap}$ holds and 0 otherwise.

As this analysis only makes sense for time periods with an actual rainfall event, we computed A_H for all n^e rainfall events in each hydrological year. More specifically, we established four A_H distributions with $n^e_{2006} = 156$, $n^e_{2007} = 192$, $n^e_{2008} = 205$, $n^e_{2009} = 219$ using a fixed number of 9 histogram classes determined after Sturges (1926).

The calculated histograms for 2006–2009 are shown in Fig. 14. A clearly observable feature is that in 2006 the number of events with more than 30% of the basin contributing to Hortonian runoff is much higher than in any other year. Beginning in 2007 the mode of the A_H distributions stabilizes at 30%, which is about the areal

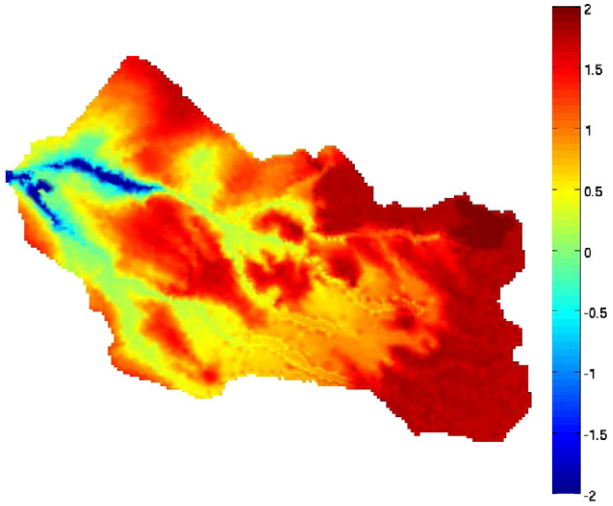

(a) $\log_{10}(Q_{ri}/Q_{cap})$ for year 2006

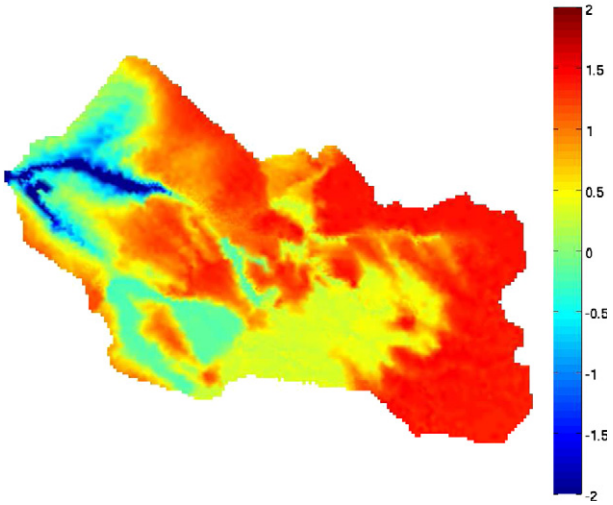

(b) $\log_{10}(Q_{ri}/Q_{cap})$ for year 2009

Fig. 15. Spatial distribution of the ratio of the input flow rate Q_{ri} and the infiltration capacity (Q_{cap}) for a typical rainfall event during the hydrological year (a) 2006 and (b) 2009.

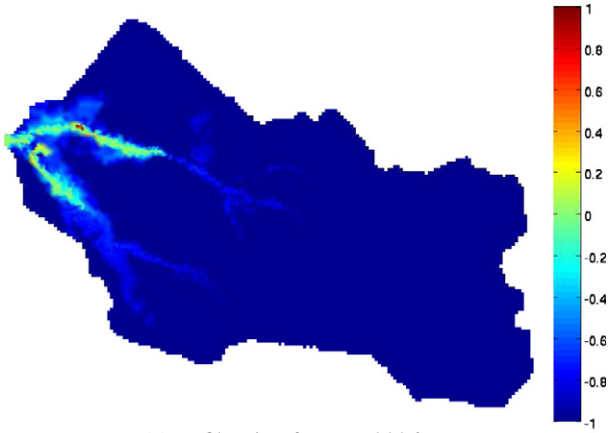

(a) Exfiltration for year 2006

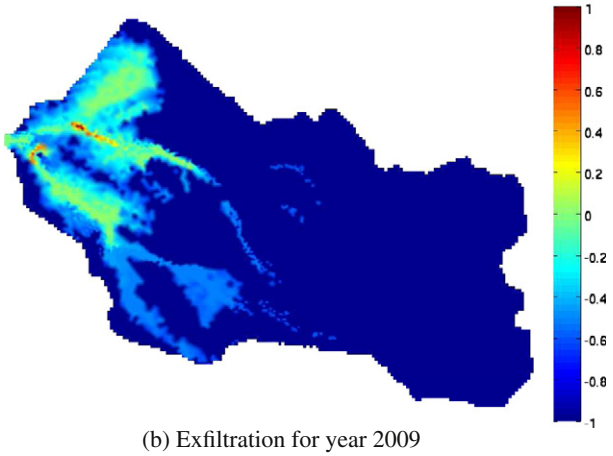

(b) Exfiltration for year 2009

Fig. 16. Exfiltration values [m/s] for a typical rainfall event during the hydrological years (a) 2006 and (b) 2009.

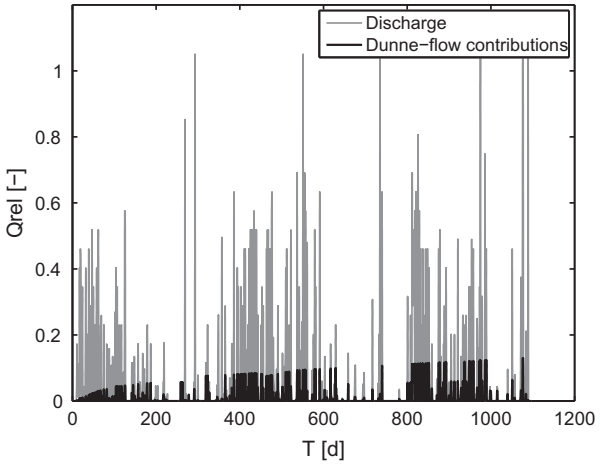

Fig. 17. Relative contributions from exfiltration (Dunne runoff) on stream discharge for hydrological years 2006–2009.

proportion of the Lerma basin that remains un-irrigated. For 2007–2009, we can hardly observe events in which Q_{cap} is exceeded in more than 70% of the total basin area, which occurred relatively frequently in 2006. Overall the distribution of 2006 seems to have lost its right tail and to concentrate frequency mass in the three lowermost classes.

While these distributions are still also a function of the actual rainfall distribution within the respective years, the similarity between 2007–2009 and their dissimilarity with 2006 further supports our conclusion that the Hortonian runoff generation process becomes less important for the Lerma basin. Furthermore, these statistics seem to indicate that Hortonian runoff generation remains mainly active in the non-irrigated part.

In order to highlight the spatial differences between 2006 and 2009 we show the catchment response to two rainfall events of similar intensity (i.e. 13.5 and 12.4 mm/h respectively). To minimize the influence of antecedent moisture conditions, we selected these events from a subset of events with 3 preceding dry days. For the two selected events, we calculated the ratio between Q_{ri} and Q_{cap} at each node. In Fig. 15 the spatial distribution of the logarithm of this ratio $\log_{10}(Q_{ri}/Q_{cap})$ is presented, so that areas with Hortonian runoff are associated with positive values. Despite the similarity of the rainfall events - both hydrological years can be well distinguished by their response: In 2006 as Q_{cap} is exceeded in 91% of the total area. In 2009, Q_{ri} only exceeds Q_{cap} in 54% of the total area and event water can infiltrate at low elevations and within intensively irrigated areas. The percentage of areas with

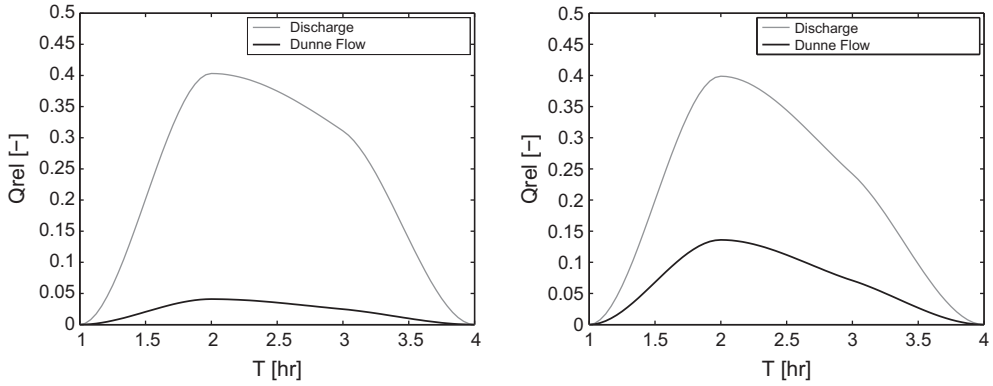

Fig. 18. Dunne overland flow and measured stream discharge for two typical rainfall events with similar intensity and duration in hydrological years (a) 2006 and (b) 2009.

Hortonian runoff generation is almost as high as the percentage of the total non-irrigated area in 2009 (≈47%). The remaining ≈7% of the former are either regions close to the discharging streams or associated with a portion of the pinetree field located in the middle of the basin. That part is not irrigated, but likely receives water from adjacent irrigated plots.

In order to support the applicability of the average approximate infiltration capacity defined in Eq. (18), we extracted the spatial distribution of fluxes exfiltrating from the subsurface domain directly from the physics-based model for the same rainfall events referred to above. Areas with exfiltrating fluxes represent areas of Dunne-runoff by definition. The results are shown in Fig. 16, where positive values represent exfiltration and negatives values represent infiltration. It can be observed that the areas associated to exfiltration correlate very well with those areas considered as Dunne-runoff areas in Fig. 15. This indicates that our approximate infiltration capacity represents a good measure to discriminate between areas of Hortonian and Dunne-runoff generation processes.

Additionally, we compare the sum of exfiltrating fluxes (i.e. the Dunne flow contribution) to the stream discharge at the Lerma basin outlet. This total exfiltration was obtained by integrating the exfiltration over the whole surface area of the Lerma basin model taking spatial differences into account and normalizing by the total precipitation:

$$\mathrm{Exf} = \frac{\int_A \frac{k_r k_{33}}{l_e}(\psi - H)\mathrm{d}A}{P} \tag{20}$$

The integration given in Eq. (20) was repeated using a 1-h time-step for the whole simulated period. Considering the size of the Lerma basin and the velocity of surface runoff it can be assumed that the error introduced by differing arrival times of exfiltrating water is small. We also neglect the effect of re-infiltration which may introduce an error for a particular event, but becomes insignificant when considering the time evolution of stream discharge and its Dunne flow contribution. The resulting curve is presented in Fig. 17. It can be observed that the contribution of Dunne flow has increased along with the intensification of the irrigation in the Lerma basin. This behavior is in agreement with the rise of dry-weather baseflow measured at the outlet of the Lerma basin and with the increase of the total length of perennial streams discussed in Section 6.2.

To further highlight the change in Dunne overland flow contribution, we present a close-up view of the hydrological response at the Lerma basin outlet for the two events used above (i.e. for hydrological years 2006 and 2009). In Fig. 18, discharge and Dunne flow contribution for these particular events are presented. Despite the similarity of the events (i.e. duration and intensity), Dunne flow represents a considerably larger portion of the measured discharge for the event in 2009 (28%) than for the event in 2006 (10%).

7. Conclusions

We have set up a physics-based fully-coupled surface–subsurface model to simulate the transformation of the Lerma basin from a non-cultivated dry land into an irrigated crop land. We strongly believe that modeling such a system requires not only accounting for surface processes but also for variably-saturated subsurface dynamics. A comparison of measured and simulated flow dynamics revealed that the model proposed is able to reproduce detailed temporal and spatial features of the flow dynamics.

Our analysis of the semi-arid Lerma basin suggests a significant influence of the van Genuchten parameters, air-entry pressure α and pore-size factor n, on the aggregated hydrological catchment response. Despite the non-uniqueness problems reported in the literature we found these parameters to be identifiable when the parameter estimation problem is constrained by a geology-guided zonation approach and a restriction to physical parameter value ranges based on texture. Nonetheless, laboratory measurements of soil water-retention curves are of course preferable, if available for similar studies.

The evolution of the total length of streams within Lerma basin show the ability of the model to reproduce detailed spatial features, in particular the change of the southern creek from intermittent to perennial, as well as the short-term effect of quick irrigation return flows on the size of the drainage network.

The evolution of the approximate infiltration capacity curve shows a raising base level due to irrigation agriculture. Our analysis shows that this can be indicative of a shift in the occurrence of Hortonian runoff generation from frequently in 2006 to episodic in 2009. Furthermore, direct consideration of exfiltrating fluxes calculated by the physics-based model show a higher contribution of Dunne flow to the stream flow at the Lerma basin outlet, which is consistent with the shift obtained from the approximate infiltration capacity concept. In that respect Lerma basin turned from a system of low interaction with the underlying aquifer into a system with a much higher groundwater-surface water interaction.

At least at the scale of the Lerma basin, the good model performance on the validation data set implies that it is possible to simulate catchment systems under land-use change with physics-based models using physically meaningful, identifiable parameter sets. Limitations of physics-based models include fairly high data requirements to describe the spatial variability of model parameters and boundary conditions. Additionally, the model used in

our investigation is computationally very demanding because of (i) the large non-linearities when solving the subsurface variably-saturated flow equations during the dry months and (ii) the small time-steps enforced during the high-intensity rainfall events. Nevertheless, Kollet et al. (2010) only recently have prepared the future track for physics-based catchment models in terms of computational feasibility.

The model presented in this study also serves as a basis for further investigations in the Lerma basin. Water quality questions will be tackled in future studies, where the model will be used to study the nitrate fate and transport in order to predict local impacts of the ongoing change towards larger irrigation-based agriculture in the Arba catchment. Additionally, the model will be used to evaluate the impact of future climate scenarios (Bürger et al., 2007) on the sustainability of irrigation agriculture within the Lerma basin.

Acknowledgments

This study has been partially funded by the ALECOL-DAAD program under the Grant A/07/03960, the Colombian Ministry of Education, Antonio Nariño University (Bogota, Colombia); the program Alban, the European Union program of High Level Scholarships for Latin America and for the Spanish Ministry of Science and Innovation (Project CGL2009–13410-C02–01) and the 6th framework program AquaTerra (contract GOCE 505428). We also thank three anonymous reviewers for their constructive suggestions.

References

Allen, R., 2005. The ASCE Standardized Reference Evapotranspiration Equation. American Society of Civil Engineers.
Allen, R., Pereira, L., Raes, D., Smith, M., 1998. Crop evapotranspiration: guidelines for computing crop water requirements. FAO Irrigation and Drainage Paper (56), FAO, Rome, Italy, p. 300.
Anderson, M., Woessner, W., 1992. Applied Groundwater Modeling: Simulation of Flow and Advective Transport. Academic Press.
Betson, R., 1964. What is watershed runoff. Journal of Geophysical Research 69 (8), 1541–1552.
Beven, K., 1979. A sensitivity analysis of the Penman–Monteith actual evapotranspiration estimates. Journal of Hydrology 44 (3/4).
Beven, K., 1989. Changing ideas in hydrology-the case of physically-based models. Journal of Hydrology 105 (1–2), 157–172.
Beven, K., 1993. Prophecy, reality and uncertainty in distributed hydrological modelling. Advances in Water Resources 16, 41–51.
Beven, K., 2001. Dalton Medal Lecture: How far can we go in distributed hydrological modelling? Hydrology and Earth System Science 5 (1), 1–12.
Beven, K., 2002. Towards a coherent philosophy for modelling the environment. Proceedings of the Royal Society of London A – Mathem and Physical and Engineering Sciences 458 (2026), 2465–2484.
Bicknell, B., Imhoff, J., Kittle, J., Donigian, A., Johanson, R., 1993. Hydrological Simulation Program-FORTRAN (HSPF): User's Manual for Release 10.0. Environmental Research Laboratory, US Environmental Protection Agency, Athens, GA. PA, 600(3), p. 84.
Bronstert, A., Bárdossy, A., 2003. Uncertainty of runoff modelling at the hillslope scale due to temporal variations of rainfall intensity. Physics and Chemistry of the Earth 28 (6–7), 283–288.
Bürger, C., Kolditz, O., Fowler, H., Blenkinsop, S., 2007. Future climate scenarios and rainfall–runoff modelling in the Upper Gallego catchment (Spain). Environmental Pollution 148 (3), 842–854.
Carsel, R., Parrish, R., 1988. Developing joint probability distributions of soil water retention characteristics. Water Resources Research 24 (5).
Causape, J., 2002. Repercusiones medioambientales de la agricultura sobre los recursos hıdricos de la Comunidad de Regantes n V de Bardenas (Zaragoza). Ph.D. thesis, Tesis Doctoral, Departamento de Ciencias de la Tierra, Facultad de Ciencias Geologicas, Universidad de Zaragoza. 153 pp. <http://www.cervantesvirtual.com>.
Causapé, J., Quílez, D., Aragüés, R., 2004. Assessment of irrigation and environmental quality at the hydrological basin level I: irrigation quality. Agricultural Water Management 70 (3), 195–209.
Causapé, J., Quílez, D., Aragüés, R., 2006. Groundwater quality in CR-V irrigation district (Bardenas I, Spain): alternative scenarios to reduce off-site salt and nitrate contamination. Agricultural Water Management 84 (3), 281–289.
Dingman, S., 2002. Physical Hydrology, vol. 1. Prentice Hall.
Downer, C., Ogden, F., 2004. Appropriate vertical discretization of Richards' equation for two-dimensional watershed-scale modelling. Hydrological Processes 18 (1), 1–22.
Dunne, T., Black, R., 1970. Partial area contributions to storm runoff in a small New England watershed. Water Resources Research 6 (5), 1296–1311.
Eagleson, P., 1978. Climate, soil, and vegetation: 1. Introduction to water balance dynamics. Water Resources Research 14 (5), 705–712.
Ebel, B., Mirus, B., Heppner, C., Vanderkwaak, J., Loague, K., 2009. First-order exchange coefficient coupling for simulating surface water–groundwater interactions: parameter sensitivity and consistency with a physics-based approach. Hydrological Processes 23, 1949–1959.
Ebel, B., Loague, K., 2006. Physics-based hydrologic-response simulation: seeing through the fog of equifinality. Hydrological Processes 20 (13), 2887–2900.
Ferguson, I., Maxwell, R., 2011. Hydrologic and land–energy feedbacks of agricultural water management practices. Environmental Research Letters 6, 014006.
Freeze, R., Cherry, J., 1979. Groundwater. Prentice-Hall, Englewood Cliffs.
Freeze, R., Harlan, R., 1969. Blueprint for a physically-based, digitally-simulated hydrologic response model. Journal of Hydrology 9 (3), 237–258.
García-Garizábal, I., Valenzuela, J., Abrahão, R., 2009. Evolution of the efficiency and agro-environmental impact of a traditional irrigation land in the middle Ebro Valley (2001–2007). Spanish Journal of Agricultural Research 7 (2), 465–473.
Garcia-Vera, M., Martinez-Cob, A., 2004. Revisin de las necesidades hdricas netas de los cultivos de la Cuenca del Ebro. Technical report, Ministerio de Medio Ambiente, Confederacin Hidrogrfica del Ebro, Oficina de Planificacin Hidrolgica.
Gottardi, G., Venutelli, M., 1993. A control-volume finite-element model for two-dimensional overland flow. Advances in Water Resources 16 (5), 277–284.
Hargreaves, G., Samani, Z., 1985. Reference crop evapotranspiration from temperature. Applied Engineering in Agriculture 1 (2), 96–99.
Horton, R., 1933. The role of infiltration in the hydrologic cycle. Transactions – American Geophysical Union 14, 446–460.
Jones, J., Sudicky, E., McLaren, R., 2008. Application of a fully-integrated surface-subsurface flow model at the watershed-scale: a case study. Water Resources Research 44 (3), W03407.
Kitanidis, P., 1997. The minimum structure solution to the inverse problem. Water Resources Research 33 (10), 2264–2272.
Kolditz, O., Delfs, J., Burger, C., Beinhorn, M., Park, C., 2008. Numerical analysis of coupled hydrosystems based on an object-oriented compartment approach. Journal of Hydroinformatics 10 (3), 227–244.
Kolditz, O., Du, Y., Burger, C., Delfs, J., Kuntz, D., Beinhorn, M., Hess, M., Wang, W., van der Grift, B., te Stroet, C., 2007. Development of a regional hydrologic soil model and application to the Beerze–Reusel drainage basin. Environmental Pollution 148 (3), 855–866.
Kollet, S., Maxwell, R., 2006. Integrated surface–groundwater flow modeling: a free-surface overland flow boundary condition in a parallel groundwater flow model. Advances in Water Resources 29 (7), 945–958.
Kollet, S., Maxwell, R., Woodward, C., Smith, S., Vanderborght, J., Vereecken, H., Simmer, C., 2010. Proof of concept of regional scale hydrologic simulations at hydrologic resolution utilizing massively parallel computer resources. Water Resources Research 46 (4), W04201.
Kristensen, K., Jensen, S., 1975. A model for estimating actual evapotranspiration from potential evapotranspiration. Nordic Hydrology 6 (3), 170–188.
Li, Q., Unger, A., Sudicky, E., Kassenaar, D., Wexler, E., Shikaze, S., 2008. Simulating the multi-seasonal response of a large-scale watershed with a 3D physically-based hydrologic model. Journal of Hydrology.
Loague, K., Heppner, C., Ebel, B., VanderKwaak, J., 2010. The quixotic search for a comprehensive understanding of hydrologic response at the surface: Horton, Dunne, Dunton, and the role of concept-development simulation. Hydrological Processes 24, 2499–2505.
Loague, K., Kyriakidis, P., 1997. Spatial and temporal variability in the R-5 infiltration data set: Deja vu and rainfall-runoff simulations. Water Resources Research 33 (12), 2883–2895.
Maier, U., DeBiase, C., Baeder-Bederski, O., Bayer, P., 2009. Calibration of hydraulic parameters for large-scale vertical flow constructed wetlands. Journal of Hydrology 369 (3–4), 260–273.
Maxwell, R., Chow, F., Kollet, S., 2007. The groundwater–land-surface–atmosphere connection: Soil moisture effects on the atmospheric boundary layer in fully-coupled simulations. Advances in Water Resources 30 (12), 2447–2466.
Maxwell, R., Kollet, S., 2008. Quantifying the effects of three-dimensional subsurface heterogeneity on Hortonian runoff processes using a coupled numerical, stochastic approach. Advances in Water Resources.
Navidi, W., 2008. Statistics for Engineers and Scientists. McGraw-Hill Higher Education.
Panday, S., Huyakorn, P., 2004. A fully coupled physically-based spatially-distributed model for evaluating surface/subsurface flow. Advances in Water Resources 27 (4), 361–382.
Penman, H., 1948. Natural evaporation from open water, bare soil and grass. Proceedings of the Royal Society of London, Series A: Mathematical and Physical Sciences 193 (1032), 120–145.
Perez, A., Abrahao, R., Causape, J., Cirpka, O., Buerger, C., 2010. Implications of diffusive wave cascading plane simulations for the study of surface water – groundwater interaction with a 3-d fully-integrated catchment model. In: XVIII International Conference on Water Resources.
Scanlon, B., Jolly, I., Sophocleous, M., Zhang, L., 2007. Global impacts of conversions from natural to agricultural ecosystems on water resources: Quantity versus quality. Water Resources Research 43 (3), W03437.
Schaap, M., Leij, F., 1998. Database-related accuracy and uncertainty of pedotransfer functions. Soil Science 163 (10), 765.

Schaap, M., Leij, F., van Genuchten, M., 2001. Rosetta: a computer program for estimating soil hydraulic parameters with hierarchical pedotransfer functions. Journal of Hydrology 251 (3–4), 163–176.
Shiklomanov, I., 2000. Appraisal and assessment of world water resources. Water International 25 (1), 11–32.
Smerdon, B., Mendoza, C., Devito, K., 2007. Simulations of fully coupled lake-groundwater exchange in a subhumid climate with an integrated hydrologic model. Water Resources Research 43 (1), W01416.
Sturges, H., 1926. The choice of a class interval. Journal of the American Statistical Association 21, 65–66.
Sun, N., Sun, N., Elimelech, M., Ryan, J., 2001. Sensitivity analysis and parameter identifiability for colloid transport in geochemically heterogeneous porous media. Water Resources Research 37 (2), 209–222.
Therrien, R., McLaren, R., Sudicky, E., Panday, S., 2008. A three-dimensional numerical model describing fully integrated subsurface and solute surface flow and solute transport. Technical report.
Van Genuchten, M., 1980. A closed-form equation for predicting the hydraulic conductivity of unsaturated soils. Soil Science Society of America Journal 44 (5), 892–898.
VanderKwaak, J., 1999. Numerical Simulation of Flow and Chemical Transport in Integrated Surface–Subsurface Hydrologic Systems. Ph.D. thesis, University of Waterloo.
VanderKwaak, J., Loague, K., 2001. Hydrologic-response simulations for the R-5 catchment with a comprehensive physics-based model. Water Resources Research 37 (4), 999–1013.
Vogel, H., Ippisch, O., 2008. Estimation of a critical spatial discretization limit for solving Richards' equation at large scales. Vadose Zone Journal 7 (1), 112.